Title

High Resolution Photoelectron Spectroscopy of H{sub 2}CO{sup +} and D{sub 2}CO{sup +}

Journal

Journal of Chemical Physics, 98(6)

Authors

Niu, B.
Shirley, D.A.
Bai, Y.

Publication Date

1992-08-01

LBL-32823
UC-401
Preprint

Lawrence Berkeley Laboratory
UNIVERSITY OF CALIFORNIA

CHEMICAL SCIENCES DIVISION

Submitted to Journal of Chemical Physics

High Resolution Photoelectron Spectroscopy and Femtosecond Intramolecular Dynamics of H_2CO^+ and D_2CO^+

B. Niu, D.A. Shirley, and Y. Bai

August 1992

Prepared for the U.S. Department of Energy under Contract Number DE-AC03-76SF00098

DISCLAIMER

LBL-32823
UC-401

High Resolution Photoelectron Spectroscopy and Femtosecond Intramolecular Dynamics of H_2CO^+ and D_2CO^+

Baohua Niu, David A. Shirley, and Ying Bai

Department of Chemistry
University of California

and

Chemical Sciences Division
Lawrence Berkeley Laboratory
University of California
Berkeley, California 94720

August 1992

This work was supported by the Director, Office of Energy Research, Office of Basic Energy Sciences, Chemical Sciences Division, of the U.S. Department of Energy under Contract No. DE-AC03-76SF00098.

High Resolution Photoelectron Spectroscopy and Femtosecond Intramolecular Dynamics of H_2CO^+ and D_2CO^+

Baohua Niu, David A. Shirley [1], and Ying Bai [2]

Department of Chemistry, The University of California at Berkeley

& Chemical Science Division, Lawrence Berkeley Laboratory

1 Cyclotron Road, Berkeley, CA 94720, USA

Abstract

High resolution helium Iα (584 Å) photoelectron spectra of H_2CO and D_2CO are reported. The present study reveals much new vibrational structure detail in the ionic first excited state of formaldehyde. Weak excitations of the ν_3 (in H_2CO) and ν_1 (in D_2CO) modes along with the strong excitations of the ν_2 mode in the ionic first excited states are fully resolved for the first time. The weak excitations of the ν_4 out-of-plane bending mode in the ionic ground and first excited states of formaldehyde cations indicate that they may have non-planar equilibrium geometries. Strong isotope effects on vibronic (vibrational) couplings are observed in the cation first and second excited states. Vibrational autocorrelation functions are calculated from the high-resolution photoelectron spectra. The correlation functions calculated for the first electronic excited states show rather slow decay rate on the femtosecond time scale. The ultrafast decay of the formaldehyde cations implied by the correlation functions calculated for the third electronic excited states suggest that dissociation and intramolecular dynamic processes are the main decay pathways.

I. Introduction

The photoelectron spectra of H_2CO and D_2CO have been the subject of extensive theoretical and experiment studies.[1-10] Most of the theoretical studies have been based on the earlier experimental studies by Turner et al.,[1] and by Baker et al..[2] The assignment of the four outermost valence states' adiabatic ionization energies (**AIEs**) by Turner et al. has been the subject of some theoretical calculations, especially on the ordering of the third and fourth ionic states. The vibrational fine structures observed in this early, lower-resolution work have been studied extensively by theoretical calculations.[3-10] The vibrational fine structures seemed well resolved and relatively simple in most of the electronic states. Their interpretation, however, has caused considerable difficulty.[1,2,11,12] Cederbaum[8] and coworkers used a many-body approach to the vibrational structures in formaldehyde, and cautioned that the vibrational coupling could be very different for different isotopic species. There were also some disagreements between the theoretical and experimental results regarding the vibrational assignments.[13]

The stability and the decay pathways, and the dynamics of the formaldehyde cations formed by photoionization in various ionic states have also been studied both theoretically and experimentally.[14-17] In a photoionization study by Guyon et al.,[14] they suggested that the decay of the first excited state $\tilde{A}\,^2B_1$ state produces the HCO^+ and CO^+ fragments. By using the correlation diagrams, they ascribed the production of the CO^+ ion to the electronic predissociation of the $\tilde{A}\,^2B_1$ state by an upper repulsive $^2A_1$ state leading to the CO^+ ($^2\Sigma^+$) + H_2 ($^1\Sigma_g^+$) asymptote at 14.1 eV. They proposed that the $\tilde{A}\,^2B_1$ state was predissociated by the ground $\tilde{X}\,^2B_2$ state, whose lowest asymptote leads to HCO^+ ($^1\Sigma^+$) + H (^2S) fragments. An ***ab initio*** calculation study by Pires et al.,[18] gave some justification and explanations about the exact decay mechanism in the experimental observations by invoking a particular type of intersections between the potential energy

surfaces (**PES**): conical intersections. The fragmentation of the H_2CO^+ in $\tilde{A}\ ^2B_1$ state has also been studied by coincidence experiments [15-19]. It was determined that at $v = 6$, the H_2CO^+ in the $\tilde{A}\ ^2B_1$ state starts to fragment and yields $CO^+ + H_2$, and at $v = 7$, D_2CO^+ in the $\tilde{A}\ ^2B_1$ starts to fragment and yields $CO^+ + D_2$. [15]

In this work, we report high-resolution helium **I**α (584 Å) photoelectron spectra of H_2CO and D_2CO. Improved resolution and effective cooling of the sample by supersonic expansion enabled us to determine the **AIE**s for the states accessible by the helium **I**α line (21.21732 eV) to a much higher accuracy, and to give new interpretations of the vibrational structures observed in all ionic states. The results agree fairly well with available theoretical calculations. The excitation of the ν_4 out-of-plane bending mode in the ionic ground and the first excited states imply that formaldehyde cations in these states might have non-planar equilibrium geometries. This was not discussed in any of the previous experimental and theoretical work. It was argued qualitatively by using the method first developed by R.S. Mulliken [20] and later by A. D. Walsh, [21,22] known as the Walsh diagram. The different vibrational progressions observed in the first and second excited states indicate strong isotope effects on vibronic (vibrational) couplings. Using the autocorrelation function formalism first discussed by Heller [23-26] for electronic photoabsorption and emission, and late by Lorquet et al. [27-29] , and by Ruščić [28b] for photoelectron spectroscopy, modified by Pollard et al. [30] and by Reutt et al., [31,32] the femtosecond ultrafast intramolecular dynamics of the formaldehyde cation in its various ionic states is discussed.

The details of the experiments are described in section II. The vibronic coupling and isotope effects on vibronic couplings are discussed briefly in section III. A description of, and the method for calculating, the autocorrelation functions are presented in section IV. Spectroscopic results and the dynamic interpretations based on the vibrational

autocorrelation functions are discussed for each of the electronic states of H_2CO^+ and D_2CO^+ in section V. The major conclusions are summarized in section VI.

B. Experiment

The molecular beam photoelectron spectrometer used for this study has been described previously [34,35] Briefly, it consists of a supersonic molecular beam source; a windowless helium discharge lamp optimized to produce only the helium Iα resonance line with minor contamination from higher resonance lines; a quadrupole mass spectrometer (QMS) to characterize the beam composition; a high-resolution electron-energy analyzer consisting of a 90° spherical sector prefilter and a 180° hemispherical analyzer equipped with a multichannel detector, and associated electron optics; and a dedicated microcomputer (LSI-11/73) for data acquisition and control. The electrons are collected at a 90° angle with respect to the incident photon beam and the supersonic molecular beam and the intensity is uncorrected for angular distribution effects. Formaldehyde ß values for helium Iα photons are not available, although there are angle-resolved photoelectron studies [33] on formaldehyde in the photon energy range 10 - 30 eV using synchrotron radiation, which gave the ß values for the $\tilde{X}\ ^2B_2$, $\tilde{A}\ ^2B_1$, $\tilde{B}\ ^2A_1$, and $\tilde{C}\ ^2B_2$ states at photon energy around 21 eV: 0.5, 0.5, 0.2, 0.3, respectively. The energy resolution was 11 meV (FWHM) as calibrated by Ar photoelectron peaks.

Approximately 300 torr of ultra high purity helium (99.9999 %, Matheson) was first passed through a U tube maintained at 77 K to remove trace amount of water in the carrier gas line, then bubbled through a liquid monomer H_2CO or D_2CO trap maintained at acetone/dry ice slush temperature (195 K) with vapor pressures about 35 torr and 30 Torr as measured with an MKS model 122AA-2000 Baratron. The monomer H_2CO or D_2CO was prepared following a literature procedure [36] by thermocracking paraformaldehyde and fully deuterated paraformaldehyde (MSD Isotopes, 99% D-atom) at ca.393 K,

fractionating (at 195 K) and trapping the monomer (at 77 K), and storing it in the dark with continuous pumping at 77 K before use. The He/H_2CO or He/D_2CO mixture with a total pressure of ca. 350 torr, was expanded through a 70 μm diameter converging molybdenum nozzle held at room temperature, and skimmed by a 0.858 mm diameter, 6.4 mm tall conical stainless steel skimmer, D_{ns} = 6.4 mm. The beam source chamber pressure was 6 x 10^{-5} torr, and the main chamber pressure was 3 x 10^{-6} torr during the experimental measurements. All gas inlet lines were minimized and extensively baked (473 K) under vacuum (10^{-7} torr) to remove trace amounts of water, which is known to catalytically polymerize formaldehyde. Beam compositions were checked using the **QMS**. No polymers of H_2CO or D_2CO were found under these experimental conditions. The rotational temperature in the beams was estimated to be <10 K as shown by laser induced fluorescence (**LIF**) measurements under similar conditions. [37]

The complete photoelectron spectrum of each isotopic species was obtained as four sequential scans of the electron kinetic energy. Each scan was preceded and immediately followed by an argon calibration scan. To enhance statistics, four complete spectra of H_2CO and D_2CO were scanned and summed. Thus the reported photoelectron bands each represents the summation of four scans. Individual scans were made within a time period of less than two hours. Restricting the length of each scan limits the total drift in the electron kinetic energy scale to ≤ 1 meV. The linearity of the kinetic energy scale was determined by obtaining the N_2^+ photoelectron spectrum and comparing the N_2^+ $\tilde{X}\,^2\Sigma_g^+$ (v=0) and $\tilde{B}\,^2\Sigma_u^+$ (v=0) splitting with the accurate literature value of 3.16981 eV available from N_2^+ optical emission spectroscopy. [38] At higher kinetic energies, the linearity of the energy scale was checked by the photoelectron spectra of argon and xenon. The ionization potential of these rare gases (I.P. Ar $^2P_{3/2}$ = 15.75975 eV, and Xe $^2P_{3/2}$ = 12.13000 eV) have been precisely determined from optical spectroscopy.[39] The linearity of the molecular beam spectrometer is within ±1.0 meV over this entire energy range. The combination of

the drift and the linearity of the energy scale errors limits the accuracy at which the absolute ionization potential may be reported to ± 3.0 meV. Other spectroscopic constants, however, are obtained as line splittings and may be reported to a much higher accuracy of ±0.5 meV (4.3 cm^{-1}).

III. Vibronic Coupling and Isotope Effects on Vibronic Coupling

In photoelectron spectroscopy, the vibronic coupling effect , i.e., the interaction of electronic and nuclear (vibrational) motion, is often invoked to explain the observation that there are vibrational progressions in modes which are not allowed by selection rules based on the **Born-Oppenheimer (BO)** approximation; [40] that the observed vibrational frequencies are very low; and that odd quanta of non totally symmetric vibrations get excited. There are other couplings and resonance effects which can also cause similar effects: vibrational-rotation coupling, rotation-electronic couplings and **Fermi** resonances. In general, these effects are much weaker than the vibronic coupling effect and are much easier to identify.

Vibronic coupling effects are usually treated as perturbations to the **B O** approximation, that is the adiabatic, Hamiltonian $\mathcal{H}_0$, [41] if we assume that the corrections caused by vibronic couplings are small in the sense that perturbation theory still can be used. We can expand the molecular Hamiltonian $\mathcal{H}(q;Q)$, which is a function of the electron q and the nuclear Q coordinates, in a Taylor series in the normal coordinates of vibration Q near the equilibrium configuration Q_0:

$$\mathcal{H} = \mathcal{H}(q;Q)_{Q_0} + \sum_{r=1}^{\infty} \left| \frac{1}{r!} \frac{\partial^r \mathcal{H}(q;Q)}{\partial Q^r} \right|_{Q_0} Q^r + \cdots \qquad (1)$$

The first term in equation (3.1), $\mathcal{H}(q;Q)_{Q_0}$, is called the zeroth-order Hamiltonian, or the

BO adiabatic Hamiltonian, and is usually expressed as $\mathcal{H}_0$. The coupling of two wave functions Ψ_k and Ψ_j can be expressed according to the matrix elements:

$$<\Psi_k|\mathcal{H}|\Psi_j> \tag{2}$$

which can be expanded with the Hamiltonian $\mathcal{H}$ of equation (1),

$$<\Psi_k|\mathcal{H}|\Psi_j> = <\Psi_k|\mathcal{H}_0|\Psi_j> + \sum_r Q_r \langle\Psi_k\left|\frac{\partial\mathcal{H}}{\partial Q_r}\right|\Psi_j\rangle +$$

$$+ \frac{1}{2!}\sum_r Q_r^2 \langle\Psi_k\left|\frac{\partial^2\mathcal{H}}{\partial Q_r^2}\right|\Psi_j\rangle + \frac{1}{2!}\sum_{rs} Q_rQ_s \langle\Psi_k\left|\frac{\partial^2\mathcal{H}}{\partial Q_r\partial Q_s}\right|\Psi_j\rangle + \ldots \tag{3}$$

The first term in equation (3) is always zero by the orthogonality relationship. Thus the necessary conditions for the vibronic coupling effects to perturb the electronic states involved are that at least one term in the equation (3) has a nonzero value and that it is not too small compared with the zeroth-order electronic states' energy separations.

The total Hamiltonian $\mathcal{H}$ of equation (1) always possesses the full symmetry (Γ_1) of the molecular point group. This is also true for $\mathcal{H}_0$, the Hamiltonian for the zeroth-order unperturbed molecule. For the coupling operators in equation (3): $\partial\mathcal{H}/\partial Q_r$ transforms as the irreducible representation of the normal coordinate Q_r, $\Gamma(Q_r)$; $\partial^2\mathcal{H}/\partial^2 Q_r$ always has at least one component that transforms as Γ_1, the full symmetry of the molecular point group; and $\partial^2\mathcal{H}/\partial Q_r\partial Q_s$ transforms as $\Gamma(Q_r)\otimes\Gamma(Q_s)$. The linear coupling integral in equation (3) will be finite if the product of the representations of all species in the integral contains the totally symmetric representation, Γ_1, that is:

$$\Gamma(\Psi_k)\otimes\Gamma(\Psi_j)\otimes\Gamma(\partial\mathcal{H}/\partial Q_r) \subset \Gamma_1. \tag{4}$$

This will enable the Q_r normal mode to couple and mix the Ψ_k and Ψ_j electronic states. If

Ψ_k and Ψ_j are degenerate states, then Q_r is the asymmetric vibrational mode that will remove the degeneracy. We can discuss the two quadratic terms in equation (3) similarly. The linear terms are usually much larger than the quadratic terms, and the quadratic terms are normally neglected when the linear terms are nonzero. In a polyatomic molecule, there could be more than one normal mode Q_r that satisfies the condition of equation (4). Those normal modes that satisfy equation (4) are called vibronically active modes. When more than one mode is vibronically active, multimode vibronic coupling effects will occur. In general, these are more complicated to deal with. Multimode vibronic coupling effects and their influence on spectroscopy have been reviewed in detail by Köppel et al. [42]

It can be seen from equation (3) that both the linear and quadratic vibronic couplings depend on the normal coordinates which are mass-dependent. It is expected that the couplings will be different for isotope-substituted compounds in the same electronic state. One important consequence of this effect is that it is possible for different vibrational modes to be excited to a different extent for isotope-substituted compounds. Theoretical calculations have shown that these effects appear in the isotope-substituted compounds. [36] The H_2CO^+ and D_2CO^+ photoelectron spectra in their first and second excited states do show this kind of behavior, and they will be discussed further in section V of this chapter.

IV. The Vibrational Autocorrelation Function

The autocorrelation function formalism description of the intramolecular dynamic process gives complementary information to the time-dependent measurements. Lorquet et al. [27-29] first demonstrated how this can be done for photoelectron bands, using the formalism of Heller. [23-26] A variation on the method of Lorquet et al. was used by Pollard et al., [30] and by Reutt et al. [31,32] to study the dynamic characteristics of intramolecular processes using supersonic molecular beam photoelectron spectroscopy. Ruščić [28b] has also given the analytical form of the vibrational autocorrelation function for photoelectron

bands under the harmonic approximation for vibrational motions.

Very recently, Remacle et al. [29] have suggested that there exists a relationship between the vibrational autocorrelation function C(t) and the population decay function **P**(t) of a particular electronic state. They defined an average population decay curve $\mathbf{P}_{av}(t)$ valid in a particular time period, and $\mathbf{C}_{av}(t)$, the average correlation function, obtainable from C(t). It was pointed out by them that for a specific excitation, the exact initial rate of decay of $\mathbf{P}_{av}(t)$ (valid up to the dephasing time T_1) is equal to the initial rate of decay of $|C(t)|^2$, and the subsequent time evolution of $\mathbf{P}_{av}(t)$ can be obtained by averaging $|C(t)|^2$ over its oscillation to give $|C_{av}(t)|^2$. To a good approximation, the average population decay curve $\mathbf{P}_{av}(t)$ can be obtained by multiplying $|C_{av}(t)|^2$ with an appropriate constant; i.e., the slopes of the two curves are the same.

The autocorrelation function can be expressed as

$$C(t) = |\langle\phi(0)|\phi(t)\rangle|. \qquad (5)$$

Here $\phi(0)$ is the initial nuclear wavefunction and $\phi(t)$ is the time evolution of this wavefunction on the excited state **PES**. C(t) represents the probability amplitude that at time ***t*** the system remains in the initially prepared state. It must be noted that the correlation function is the measure of the time evolution of the initial wave packet on the excited state **PES** and not a measure of the excited state population. But as mentioned in the preceding paragraph, the initial decay rate of C(t), through $|C(t)|^2$, is the same as the average population $\mathbf{P}_{av}(t)$ initial decay rate. It is dominated by the dephasing of the initial wave packet due to the different shape of the excited-state **PES.** Only at times greater than a vibrational period will radiationless decay processes appear in the time evolution of the correlation function. The derivation of the autocorrelation function C(t) from photoelectron spectroscopy experimental data has been reported; only the principal points will be outlined

here. The form of photoionization cross section under the strict **Franck-Condon** approximation [40] can be expressed as

$$\sigma(E) \propto |M_{el}(Q,E)|^2 |\langle \Psi'' | \Psi' \rangle|^2| \qquad (6)$$

Here $\mathbf{M}_{el}(Q, E)$ is the pure electronic transition moment, a function of the nuclear coordinates Q and electron kinetic energy E, and Ψ'' and Ψ' are the initial- and final-state vibrational wave functions. The electronic transition moment varies slowly over the photoelectron band. In lieu of any arbitrary approximation, a constant value was used in calculating the correlation functions reported here.

Applying the completeness on a set of eigenstate Ψ'' of the molecular Hamiltonian and invoking the analytical form of the Dirac δ function, it has been shown [28a] that the cross section of photoionization becomes

$$\sigma(E) \propto \frac{1}{2\pi} \int_{-\infty}^{+\infty} e^{iEt/\hbar} \langle \Psi'' | e^{-i\mathcal{H}t/\hbar} | \Psi'' \rangle \, dt \qquad (7)$$

Here $\mathcal{H}$ is the molecular Hamiltonian, Ψ'' is identified as the initial nuclear wave function $\phi(0)$, and $e^{-i\mathcal{H}t/\hbar}|\Psi''\rangle$ is the nuclear wave function at time t: $\phi(t)$. This gives

$$\sigma(E) \propto \frac{1}{2\pi} \int_{-\infty}^{+\infty} e^{iEt/\hbar} \langle \phi(0) | \phi(t) \rangle \, dt \qquad (8)$$

and the correlation function can be obtained by a **Fourier** transformation of the cross section

$$C(t) = |\langle\phi(0)|\phi(t)\rangle| \propto \frac{1}{2\pi} \int_{-\infty}^{+\infty} \sigma(E)\, e^{-iEt/\hbar}\, dt \qquad (9)$$

This shows that the correlation function can be obtained from the **Fourier** transform of the photoelectron partial cross section $\sigma(E)$. It can be accomplished by deconvoluting the instrument response function $\mathbf{I}(E)_{ir}$, which we determine from the photoelectron spectrum of a rare gas at a kinetic energy comparable to the band of interest, from the quantity **I**(E), intensity vs. energy, which we measure in photoelectron spectroscopy. The contributions of the finite rotational temperature in a supersonic molecular beam experiment (typically ~ 5-10 Kelvin) and the rotational excitations contribution to the correlation function were removed by convoluting $\mathbf{I}(E)_{ir}$ with a gaussian function $\mathbf{I}(E)_g$ to generate a rotationally broadened instrument response function. The width of the gaussian function was chosen from the average rotational constant , $\mathbf{B}_{avg}$, of the molecular cations for the particular electronic state (if available), the finite rotational temperature, and the rotational selection rules for photoionization. Ruščić [28b] has taken a different approach to account for these corrections. However, both methods give essentially the same results in the time window of interest.

The procedure for calculating the correlation function of $\tilde{X}$, $\tilde{A}$, $\tilde{B}$, and $\tilde{C}$ states of formaldehyde and d_2-formaldehyde cations is the following. First, the band of interest was isolated (in the case of B and C states, they were digitally separated to remove the overlapping of these two bands), and the empirically determined background, plus any constant background, was then removed. The resulting band was then normalized (area = 1) and **Fourier** transformed using a discrete **FFT** algorithm. [43] The instrument response function was similarly normalized and convoluted with a Gaussian of 6.5 meV (**FWHM**). The resulting function was **Fourier** transformed and divided into that of the data. Finally,

the modulus of the previous result was calculated, which gave the correlation function. The procedure can be summarized by the following equation:

$$C^{vib}(t) = |\langle\phi(0)|\phi(t)\rangle| = \left| \int_{-\infty}^{+\infty} I(E)\, e^{-iEt/\hbar}\, dE \right| \div \left| \int_{-\infty}^{+\infty} I(E)_{ir}\, e^{-iEt/\hbar}\, dE \; X \int_{-\infty}^{+\infty} I(E)_{g}\, e^{-iEt/\hbar}\, dE \right| \qquad (10)$$

Then $|C(t)|^2$ was calculated, and $|C_{av}(t)|^2$ was evaluated by fit $|C(t)|^2$ with an exponential curve of the form Ae^{-ikt} for both the initial and the subsequent decays after the first 'vibrational' period.

V. Results and Discussions

The full spectra of H_2CO and H_2CO obtained by combining four separate scans with a resolution of 11 meV **FWHM** are shown in Figure 1. Table I summarizes the measured spectroscopic constants together with results reported in the literature. [47,48] The designations of the ionic states assume that the ions have C_{2V} symmetry. Each of the four ionic states observed will be discussed separately below.

A. First Band, the $\tilde{X}\ ^2B_2$ state

The ground states of both H_2CO^+ and D_2CO^+ have well-resolved vibrational fine structures, as shown separately in Figure 2. Observed spectroscopic results are presented in Table II. In the present work, effective rotationally cooling enables all of the observed vibrational levels to be determined with much improved accuracy and the mean energies of these transitions were determined by the following least-squares fitting procedure. The adiabatic transitions (or the most intense feature) were first determined by fitting these

features to Gaussians. The adiabatic peaks were then isolated and used as empirical functions to fit the successive vibrational levels. This procedure allows the values of peak splittings to be determined to an accuracy of $\leq \pm 0.5$ meV(ca. 4.3 cm^{-1}). The mean transition energies located through this procedure are listed for each of the bands observed in Table II. The vibrational levels for each normal mode were then least-squares fitted to the standard energy level expression of a **Morse** oscillator [46a,46b]

$$G_i^0(v) = \omega_i^0 v - \omega_i^0 x_i^0 v^2$$

with the zero point energy being set to zero, ω_i^0 and $\omega_i^0 x_i^0$ are related to ω_i and $\omega_i x_i$ in the following ways: $\omega_i = \omega_i^0 + \omega_i^0 x_i^0$ and $\omega_i^0 x_i^0 = \omega_i x_i$. Here ω_i is the fundamental vibration frequency in cm^{-1} and $\omega_i x_i$ is the quadratic anharmonicity constant for the ith normal vibrational mode.

From the results, we conclude not only that all three totally symmetric vibrational modes were excited (this agrees with the theoretical calculations by Domcke et al., [8] but not with the results of the calculations by Takeshita [13]), but also that the non-totally symmetric mode ν_4 was excited. The excitation of odd quanta of the ν_4 mode is an indication that the molecular cations might have non-planar equilibrium geometry. This can be argued qualitatively using the Walsh diagram approach. It compares very favorably with the electronic absorption spectrum correspond to the transition of $\tilde{A}\ ^1A_2 \leftarrow \tilde{X}\ ^1A_1$. In the photoelectron spectrum, this corresponds to the removal of an electron from the b_2 (n_O) orbital, thus reducing the stabilization energy gained by having two electrons in the planar form. This also reduces the repulsion between the hydrogen atoms and the oxygen atom. Molecular orbital (**MO**) theory calculations [13,44] have indicated that in the $\tilde{X}\ ^2B_2$ state of the H_2CO^+ the HCO angle decreases slightly (~ 5°) from the neutral molecular $\tilde{X}\ ^1A_1$ state. From their ***ab initio*** calculation results [45], Buenker and Peyerimhoff concluded that

molecules with 10 and 11 valence electrons are less strongly planar compared to those with 12 upon removal of electrons from the n non-bonding orbitals. But we expect the deviation from the planar equilibrium geometry to be small.

The vibrational progressions in the observed spectra confirmed the earlier ***ab initio*** calculations with a many-body approach by W. Domcke et al., [8] but disagree with the ***ab initio*** calculations by Takeshita [13] concerning the excitation of the ν_1 mode. The anharmonicity would be too big for ν_2 if we assign the feature that appeared at 11.2086 eV to be the $\nu_2 = 2$ peak, according to Takeshita. It is noteworthy that different vibrational modes get excited to different extents between formaldehyde and deuterated formaldehyde. This gave some indications that the ionic ground-state **PES** could be quite different for these isotopic compounds even if the neutral ground-state **PES** might not be much different.

The vibrational autocorrelation functions calculated using the formalism and procedure described in section IV for the $\tilde{X}\ ^1B_2$ states of H_2CO^+ and D_2CO^+ are presented in Figure 3. The complex beat pattern of the $|C(t)|^2$ curve is the result of the excitation of four different vibrational modes, after the initial drop, all having different phase and probably all having different phase space distances to travel as well. But the overall monotonic decay trend in these $|C(t)|^2$ curves does indicate that the $\tilde{X}\ ^1B_2$ state is in a stable configuration in the **Franck-Condon** region accessible by the photoionization event. It should be noticed that there were no deep minima in the correlation functions, which are characteristic of a wave packet prepared through a predominately adiabatic transition. The initially prepared wave packet is mostly localized around the minimum of the upper **PES**, and weakly oscillates around this region, retaining substantial correlation at all times. The absence of the return of major oscillation strength can be attributed to the excitation of many modes, all having different phases after the initial drop and all having

different phase spaces to travel. The calculated $|C_{av}(t)|^2$ were also present as dot lines in the figure. They were obtained by first fitting the initial drop to the form $A_i e^{-k_i t}$ where $A_i \equiv 1.000$ as the initial conditions and k_i were varied in the fit, and fitting the late drop to the form $A_f e^{-k_f t}$, where both A_f and k_f were varied. Then the total curve were obtained by setting $A_i = 1.0 - A_f$, and $|C_{av}(t)|^2 = A_i e^{-k_i t} + A_f e^{-k_f t}$. Derived A and k values for the $\tilde{X}\ 1^2B_2$ states are presented in Table II.

B. Second Band, the $\tilde{A}\ ^2B_1$ State

The second bands of H_2CO^+ and D_2CO^+ are shown in Figure 4. The vibrational progressions observed are summarized in Table III. Here the small $N_2^+ \tilde{X}\ ^2\Sigma_g^+$ (v=0) peak presented in the D_2CO^+ spectrum, resulting from the main chamber background, makes the absolute IEs reportable to an accuracy of ±1.0 meV, limited only by the energy scale drift during the scan, which lasting about two hours as discussed in section II. It should be noted that the vibrational couplings are different for H_2CO^+ and D_2CO^+. In H_2CO^+, the major vibrational excitation is the ν_2 mode, together with several quanta of ν_3 excited as well. In D_2CO^+, on the other hand, the major vibrational excitation is the ν_2 mode, but the coupling is different between vibrational modes: here it is the ν_1 mode that gets excited along with the major excitation of the ν_2 mode. These agree fairly well with the theoretical calculations by Domcke et al. [8] when many-body effects are included, but show some disagreements with the ***ab initio*** calculations by Takeshita with a **Roothaan**'s restricted **Hartree-Fork** approach. In Domcke et al.'s calculation for both isotopic species, the coupling of the ν_2 modes are very strong. They are 2.792 and 2.611 for H_2CO^+ and D_2CO^+, respectively. The coupling of ν_3 (0.270) is much stronger than that of ν_1 (0.036) in H_2CO^+, while in D_2CO^+ the coupling of ν_1 (0.414) is much stronger than that of ν_3 (0.011). Also, the lengths of the vibrational progressions are slightly different: H_2CO^+ has a slightly shorter progression than D_2CO^+ (in the case of D_2CO^+, the $\tilde{A}$ state

vibrational progression would extend to $\nu_2 = 10$ if it were not obscured by the $N_2^+ \tilde{X}\ ^2\Sigma_g^+$ (v=0) state peak). This is an indication that the ionic **PES** are slightly different for different isotopic compounds along the Q_2 normal coordinate.

The difference in vibrational excitations has its origin in the different vibronic coupling coefficients (also called vibrational couplings by Domcke et al. [8]) for the isotopic compounds as discussed in section III. As pointed out by Domcke et al. [8] in their ***ab initio*** many-body calculations, the vibrational coupling can be very different for isotopic compounds, since the coupling coefficients are mass-dependent (the kinematic matrix, which transforms from normal to internal coordinates, of D_2CO differs considerably from that of H_2CO. It is expected that different vibrational modes will be excited to different extent for isotopic molecules. This also indicates that parts of the ionic **PES** of the $\tilde{A}\ ^2B_1$ state accessible by the photoionization excitation for H_2CO^+ and D_2CO^+ are different, especially along different normal coordinates.

The strong excitation of the ν_2 mode is an indication that a strongly bonding electron is being ejected. This agrees with previous experimental and theoretical results. But the appearance of the odd ν_4 mode with very weak intensity, just as in the ionic ground state, is an indication that the molecular ions might have a nonplanar equilibrium geometry in the $\tilde{A}\ ^2B_1$ state. This could be especially important in D_2CO^+, where the $\nu_4 =$ 1, 2 peaks are comparably stronger than in H_2CO^+. Just as in their ionic ground states, the deviation from the planar equilibrium geometry in the $\tilde{A}\ ^2B_1$ state is expected to be small.

The vibrational autocorrelation functions for the $\tilde{A}\ ^2B_1$ state of H_2CO^+ and D_2CO^+ after making corrections for the instrument response function and rotational broadening, are shown at the tops of Figure 5 and Figure 6. The overall shapes of the correlation function for H_2CO^+ and D_2CO^+ are very similar, showing only one major progression with a period of about 28.5 fs, which is the vibrational period of the ν_2 mode. But the

differences are to be noted as well. In the case of H_2CO^+, the correlation function retains its major oscillation up to about 170 fs. Beyond that, the wave packet spreads out and multiple peaks appear in the correlation function. In D_2CO^+, the correlation function retains its major oscillation up to almost 300 fs. The correlation strength in C(t) is also much smaller in H_2CO^+, ~ 0.58, compared with D_2CO^+, ~ 0.74. Also, the peaks in the D_2CO^+ correlation function are much sharper than those in the H_2CO^+ correlation function. The observed differences in the appearance of the correlation function gave us some indications about the differences in the ionic **PES** between H_2CO^+ and D_2CO^+. First, the anharmonicity, which is known to cause the spreading of the correlation function peaks, must be smaller in D_2CO^+ than in H_2CO^+ along the Q_2 normal coordinates. In fact the calculated anharmonicity constants are 10.0 (±4.3) cm^{-1} and 5.7 (±4.3) cm^{-1} for H_2CO^+ and D_2CO^+, respectively, from the present study. Second, D_2CO^+ in the $\tilde{A}\ ^2B_1$ state is more tightly bound than H_2CO^+: the correlation function of D_2CO^+ retains a higher degree of correlation for longer times. This could also imply that the initial wave packet of D_2CO^+ spans a relatively smaller portion of the phase space on the upper potential energy surface.

The modulations of the correlation function were caused by two sources. The first one is the small spin-orbit splittings in this band, since it is a π bonding electron that was ejected. The **FWHM** for peaks in this band was close to 12.5 meV, which implies that the spin-orbit splitting is ≤ 2 meV. The second is the excitation of additional vibrational modes other than ν_2 in both D_2CO^+ and D_2CO^+. This gives the doublet- and multiplet-like structures in the photoelectron spectra which produce beat patterns that modulate the correlation function. After removing these two effects by the method of Lorquet, [28a] which involved dividing the C(t) obtained with $|\cos(\Omega t/2\hbar)|$, the values of Ω were chosen to give an overall monotonic decay C(t) after carefully removing the singular points in the cosine

functions by replacing all values that are smaller than $\frac{1}{2}(|\cos(\Omega t/2\hbar)|)$ with $\frac{1}{2}(|\cos(\Omega t/2\hbar)|)$. The corrected vibrational autocorrelation functions of the $\tilde{A}\ ^2B_1$ state of H_2CO^+ and D_2CO^+ are shown at the bottom of Figure 5 and Figure 6 in forms of $|C(t)|^2$. The $|C_{av}(t)|^2$ fittings of the $|C(t)|^2$ were also included there.

It can be seen from Figure 5 and Figure 6 that the overall decay behaviors of H_2CO^+ and D_2CO^+ in the $\tilde{A}\ ^2B_1$ state are very similar, but the isotope effect does manifest itself in that D_2CO^+ has a relatively slower decay rate after the initial dephasing than H_2CO^+, and the initial dephasing rates are different as well. As pointed by Ruščić [28b], this initial (before the first half vibrational period) dephasing rate depends very sensitively on the differences between the ionic state and the neutral ground-state equilibrium geometries. This is yet another possible indication that, in the $\tilde{A}\ ^2B_1$ states of H_2CO^+ and D_2CO^+, the equilibrium geometries might be slightly nonplanar. The wave packet is displaced substantially from the minimum of the upper **PES** which is consistent with the observed long vibrational progressions, indicating a strongly bonding electron being ejected. The wave packet oscillated with large amplitude on the upper **PES,** which accounts for the deep minima in the correlation functions. The time window over which we could deduce useful information on the intramolecular dynamics was limited by the finite resolution achievable. As shown in this state after removal of all the possible broadening effects, the time window was about 200 to 300 fs wide. This corresponds to an effective resolution of ≤ 2 meV, which is very close to the helium **I**α resonance line width produced by the lamp used, estimated to be ≤ 2 meV.

C. Third Band, the $\tilde{B}\,^2A_1$ State

The third bands of H_2CO^+ and D_2CO^+ are shown in Figure 7. The vibrational progressions observed are summarized in Table IV. The presence of the small Ar^+ peaks in this band, resulting from the main chamber background from frequent calibration runs, makes the absolute IEs for this band reportable to an accuracy of ±1.0meV, the same as discussed earlier in the $\tilde{A}\,^2B_1$ band of D_2CO^+. As we have pointed out in the discussion of the $\tilde{A}\,^2B_1$ band, the vibrational couplings are different for different isotopic compounds. In previous experimental and theoretical studies, it was concluded that the simplicity of this band in H_2CO^+ was due to the accidental degeneracy of the ν_2 and ν_3 normal vibrational modes. The removal of this degeneracy in D_2CO^+ was used as evidence for this interpretation.

The ν_2 vibrational frequency is 1304.5 cm^{-1} for H_2CO^+ and 1311.1 cm^{-1} for D_2CO^+ from the present study. The ν_3 vibrational frequency, as determined from this band of D_2CO^+, is 957.4 cm^{-1}, for H_2CO^+ is 1304.5 cm^{-1} (assuming here $\nu_3 = \nu_2$). This reduction upon deuteration seems reasonable when compared with the neutral $\tilde{X}\,^1A_1$ ground state of H_2CO and D_2CO with ν_3 = 1500.2 cm^{-1}, and 1105.7 cm^{-1} respectively. The FWHM in the spectra shown for H_2CO^+ and D_2CO^+ is about 12 meV, which is very close to the measured instrumental resolution. Unless ν_2 and ν_3 were truly degenerate to within 1 meV or less, we would have seen a broadening of the peaks in the H_2CO^+ spectrum. Upon close examination, it is the other way around, however: the peaks in D_2CO^+ are slightly broader than those in H_2CO^+. Theoretical calculations [8] indicate that in the $\tilde{B}\,^2A_1$ state of H_2CO^+, the coupling of ν_3 (0.301) is much weaker than that of ν_2 (1.156). In D_2CO^+, the coupling of ν_3 is slightly larger (0.855) than that of ν_2 (0.765) when many-body effects are included, according to these authors. It is possible that the coupling of ν_3 in the $\tilde{B}\,^2A_1$ state of H_2CO^+ is so weak that we are actually seeing only the

progression of the ν_2 vibration. While in the $\tilde{B}\,^2A_1$ state of D_2CO^+ both ν_3 and ν_2 are coupled strongly, both vibrational progressions are seen. We thus tentatively assigned the vibrational progressions in the $\tilde{B}\,^2A_1$ state of H_2CO^+ to the ν_2 mode only. The present assignment and the observed **AIEs**, and vibrational progressions definitely support the assignment of Brundle et al. [12] and all theoretical calculations [3-13] available: i.e., that this band is the $\tilde{B}\,^2A_1$ state of formaldehyde.

The vibrational correlation functions for the $\tilde{B}\,^2A_1$ state of H_2CO^+ and D_2CO^+, calculated by digitally removing the $\tilde{C}\,2^2B_2$ bands' contributions, are shown in Figure 8. It can be seen from Figure 8 that for H_2CO^+, there is only one major progression, with a period of ~ 40 fs. The anharmonicity starts to spread the correlation function around t = 100 fs. The slow decay of the correlation function indicates that this state is in a very stable configuration regarding deformations along the Q_2 normal coordinate. In the case of D_2CO^+, it can be seen that this state is in a very stable configuration regarding deformations along both the Q_2 and the Q_3 normal coordinates. The overall rate of decay, as shown by the $|C_{av}(t)|^2$ of both isotopic compounds, is very similar qualitatively. Quantitatively speaking, in this electronic state D_2CO^+ is more stable than H_2CO^+. In D_2CO^+, the excitations of both the ν_2 and ν_3 modes give rise to the doublet- and multiplet-like structures in the photoelectron spectrum. These doublet and multiplet structures in the energy domain, when **Fourier** transformed, give rise to the beat pattern observed in the correlation function, as discussed in the previous section, and was not corrected for this band. It is to be noted here that the initial rates of decay for H_2CO^+ and D_2CO^+ in this state are very different, indicating again possibly different **PES** for H_2CO^+ and D_2CO^+ in the $\tilde{B}\,^2A_1$ state. The deep valleys in the correlation functions, as discussed in the previous section on the $\tilde{A}\,^2B_1$ state correlation function, indicate a substantially displaced wave packet from the upper potential energy minima.

D. Fourth Band, the $\tilde{C}\ 2^2B_2$ State

The fourth band of H_2CO^+ was shown in Figure 7, together with the $\tilde{B}\ ^2A_1$ state. The $\tilde{C}\ 2^2B_2$ state of D_2CO^+ is shown separately in Figure 9. Even with supersonic cooling in the present high-resolution study, the complexity of this band for both H_2CO^+ and D_2CO^+ cannot be fully untangled. The vibrational assignment could only be regarded as tentative, especially in the case of D_2CO^+. As pointed out by Turner et al. in their original studies, this complexity might have been caused by the crossing of another repulsive state with the $\tilde{C}\ 2^2B_2$ state. Theoretical calculations do indicate that the density of the electronic states increases rapidly with electronic energy. In the energy range of 16.4-17 eV (where the fourth band appears in the photoelectron spectrum) above the ground state of the neutral molecule, four electronic states are present and their **PES** intersect. [18] In H_2CO^+, the major progressions are assigned to the excitations of ν_1 and ν_3 modes, based largely on the many-body calculations by Domcke et al. [8] The adiabatic ionization potential was tentatively assigned as **AIE** = 16.2395(±0.003) eV. In D_2CO^+, the major vibrational progressions are much weaker compared with the corresponding ones in H_2CO^+, and were assigned to ν_1, ν_2, and ν_3 modes. The adiabatic ionization potential, however, can only be estimated to be $\leq 16.435 \pm 0.02$ eV.

The vibrational correlation functions for the $\tilde{C}\ 2^2B_2$ state of H_2CO^+ and D_2CO^+ are presented in Figure 10. The major feature of the correlation functions for this band is the extremely fast loss of correlation strength as manifested by the correlation functions obtained. Beyond the initial drop of the correlation function at ~ 5 fs, there are no recognizable major oscillations that are above noise level. This and the appearance of the broad photoelectron bands indicate that the molecular ions created by the photoionization event in this state undergo very fast intramolecular dynamic processes. The wave packet never regains its initial shape by returning to its initial position on the upper **PES**. Even

the initial drop in the correlation function is much faster when compared with other bands of these molecular ions. This, in the spirit of Ruščić, [28b] indicates that the ionic state equilibrium geometry is substantially different from not only the ground-state equilibrium geometry of the neutral molecule, but also other ionic electronic states as well. Isotope effects showed up strongly here: the correlation strength of H_2CO^+ drops much faster than that of D_2CO^+.

VI. Conclusions

Rotationally cold photoelectron spectra of H_2CO and D_2CO with much improved resolution have allowed each of the four ionic electronic states accessible by the helium **I**α radiation to be characterized in more detail. The assignment of the third and fourth ionic states to the $\tilde{B}\ ^2A_1$ and $\tilde{C}\ 2^2B_2$ states confirms the results of Brundle et al., and all theoretical calculations available. For the $\tilde{X}\ 1^2B_2$ and the $\tilde{A}\ ^2B_1$ states, the excitation of odd quanta of the non totally symmetric vibrational mode (ν_4) indicates the possibilities of nonplanar equilibrium geometries for these two states. Strong isotope effects were observed in the vibronic couplings in the $\tilde{A}\ ^2B_1$ and $\tilde{B}\ ^2A_1$ states, where very different vibrational progressions were observed in the same electronic state for different isotopic compounds. This indicates that for isotopic compounds the details of the ionic **PES** for the same electronic state can be different. Rotationally resolved spectroscopic studies on H_2CO^+ and D_2CO^+ in its various ionic states will be very desirable to confirm the equilibrium geometries of these molecular cations.

Vibrational correlation functions were derived for all four electronic states. The variations between the isotopic species' correlation functions were attributed primarily to the differences in the details of the **PES** and in the phase space spanned by the initially formed wave packets. Ultrafast intramolecular decay mechanisms were evident for the $\tilde{C}\ 2^2B_2$ state of each isotopic cation. The decaying of this state occurred on a time scale of

less than one period of C-H stretching vibrational, supporting the relaxation pathways by predissociation and through curve crossing by close-lying and intersecting electronic states in that energy range. Further theoretical treatment on this state will be particularly important to understand the details of the ultrafast intramolecular dynamics evident in the present investigation.

Acknowledgment

This work was supported by the Director, office of Energy Research, Office of Basic Energy Sciences, Chemical Science Division of the U.S. Department of Energy under Contract No. DE-AC03-76SF00098.

1. Present Address: The Pennsylvania State University, 114 Kern Graduate Building, University Park, PA 16802, USA.

2. Participating guest, permanent address: Department of Chemistry, Jilin University of Technology, Changchun, Jilin, The People's Republic of China.

References:

1. A. D. Baker, C. Baker, C. R. Brundle, and D. W. Turner, Int. J. Mass Spectrom. Ion Phys., **1**, 285(1968)
2. D. W. Turner, A. D. Baker, and C. R. Brundle, **Molecular Photoelectron Spectroscopy**, John Wiley & Sons, London, p135-137(1970)
3. W. V. Niessen, G. Bieri, and L. Åsbrink, J. Elect. Spect. Relat. Phenom. **21**, 175(1980)
4. K. Kimura, S. Katsumata, Y. Achiba, T. Yamazaki, and S. Iwata, **Handbook of HeI Photoelectron Spectra of Fundamental Organic Molecules**, Halsted, New York, (1981)
5. D. P. Chong, F. G. Herring, and D. Mcwilliams, J. Chem. Phys., **61**, 958(1974)
6. L. S. Cederbaum, G. Hohlneicher, and W. V. Niessen, Mol. Phys., **26**, 1405(1973)
7. L. S. Cederbaum, and W. Domcke, J. Chem. Phys., **64(2)**, 603(1976)
8. D. Domcke, and L. S. Cederbaum, ***ibid***, **64(2)**, 612(1976)
9. J. F. Blanke, and J. Overend, in **Vibrational Spectra and Structure**, **Vol. 7**, p270-315(1978), ed. by J. R. Durig, Elsevier Sci. Pub. Com., New York

10a. D. C. Moule, **Vibrational Spectra and Structure**, **Vol. 6**, p228-271(1977), ed. by J. R. Durig, Elsevier Sci. Pub. Com., New York.

10b. I. W. Levin, and R. A. R. Pearce, in **Vibrational Spectra and Structure**, **Vol. 4**, ed. by J. R. Durig, Elsevier Sci. Pub. Com., New York, p102(1975).

11. C. R. Brundle, and D. W. Turner, **Chem. Comm.**, 341(1967)
12. C. R. Brundle, M. B. Robin, N. A. Kuebler, and H. Basch, J. Am. Chem. Soc., **94**, 1451(1972)
13. K. Takeshita, J. Chem. Phys., **94(11)**, 7259(1991)
14. P. M. Guyon, W. A. Chupka, J. Berkowitz, *ibid*, **64**, 1419(1976)

15. R. Bombach, J. Dannacher, J-P Stadelmann, and J. Vogt, Chem. Phys. Lett., **76(3)**, 429(1980)

16. S. V. Andreyev, V. S. Antonov, I. N. Knyazev, and V. S. Letokhov, Chem. Phys. Lett., 45(1), 166(1977).

17. R. Bombach, J. Dannacher, J-P Stadelmann, and J. Vogt, Int. J. Mass Spectrom. Ion Phys., **40**, 275(1981).

18. M. Van Pires, C. Galloy, and J. C. Lorquet, J. Chem. Phys., **69**, 3242(1978).

19. S. T. Hood, A. Hamnett, and C. E. Brion, Chem. Phys. Lett., **41(3)**, 428(1976).

20. R. S. Mulliken, Rev. Mod. Phys., **14**, 204(1942).

21a. A. D. Walsh, **J. Chem. Soc.**, 2260(1953).

21b. D. C. Moule, A. D. Walsh, Chem. Rev., **75(1)**, 67-84(1975).

22. R.J. Buenker, S.D. Peyerimhoff, Chem. Rev., **74(2)**, 127-188 (1974).

23 E. J. Heller, J. Chem. Phys., **68**, 2066(1978).

24. E. J. Heller, E. B. Stechel, M. J. Davis, *ibid*, **73(10)**, 4720(1980).

25. E. J. Heller, Acc. Chem. Res., **14**, 368(1981).

26. E. J. Heller, R. Sundberg, and D. Tanner, J. Chem.. Phys., **76**, 1822(1982).

27. B. Layh-Nihaut, and J. C. Lorquet, *ibid*, **88(9)**, 5606(1988).

28a. A. J. Lorquet, J. C. Lorquet, J. Delwiche, and M. J. Hubin-Franskin, *ibid*, **76(10)**, 4692(1982).

28b. B. Ruščić, *ibid*, **85(7)**, 3776(1986).

29. F. Remacle, M. Desoute-Leconmte, and J. C. Lorquet, *ibid*, **91(7)**, 4155(1989).

30. J. E. Pollard, D. J. Trevor, J. E. Reutt, Y. T. Lee, and D. A. Shirley, *ibid*, **81(2)** 5302(1984).

31. J. E. Reutt, L. S. Wang, J. E. Pollard, D. J. Trevor, Y. T. Lee, and D. A. Shirley, *ibid*, **84(6)**, 3022(1986).

32. J. E. Reutt, L. S. Wang, Y. T. Lee, D. A. Shirley, *ibid*, **85(12)**, 6928(1986).

33. P. R. Keller, J. W. Taylor, F. A. Grimm, and T. A. Carlson, Chem. Phys., **90**, 147-153(1984).

34a. J. E. Pollard, D. J. Trevor, Y. T. Lee, and D. A. Shirley, Rev. Sci. Instrum., **52**, p1837 (1981).

34b. J. E. Pollard, Ph.D. Thesis, Department of Chemistry, The University of California at Berkeley (1982).

35. J. E. Reutt, Ph.D. Thesis, Department of Chemistry, The University of California at Berkeley (1986).

36a. R. Spencer, and W. Wild, **J. Chem. Soc.**, London, 338-340(1935).

36b. R. Spence, and W. Wild, **J. Chem. Soc.**, London, 506-509(1935).

37. W. E Polik, Ph.D. Thesis, Department of Chemistry, The University of California at Berkeley (1988)

38. A. Lofthus, and P.H. Krupenie, J. Phys. Chem. Ref. Data, **6**, 113 (1977)

39. Atomic Energy Levels, Vol. I, II, III, ed. by C. E. Moore, (National Bureau of Standards, Washington D.C., 1958).

40a. M. Born, J.R. Oppenheimer, Ann. Phys.(Lepzig), **84**, 457-484 (1927).

40b. M. Born, Nachr. Akad. Wiss. Gottingen, Math.-Phys. **KL**, IIa, P1 (1951).

40c. M. Born, K. Huang, Dynamics of Crystal Lattice, Oxford U. Press, NY., (1954).

41. J. W. Rabalais, **Principles of Ultraviolet Photoelectron Spectroscopy**, John Wiley & Sons, New York (1979)

42. H. Köppel, W. Domcke, and L. S. Cederbaum, **Adv. Chem. Phys.**, Vol. LVII, p59-246(1984)

43. E. Oran Brighan, The Fast Fourier Transform, (Prentice-Hall, Englewood Cliffs), p164(1974).

44. R. J. Buenker, and S. D. Peyerimhoff, Chem. Rev., **7(2)**, 127-188(1974)

45. R. J. Buenker, and S. D. Peyerimhoff, J. Chem. Phys., **53**, 1368(1970)

46a. J. I Steinfeld, **An Introduction to Modern Molecular Spectroscopy**, 2nd ed., The **MIT** Press, Cambridge, MA(1985) p133.

46b. G. Herzberg, **Molecular Spectra & Molecular Structure**, **I. Spectra of Diatomic Molecules**, Van Norstrand Reinhold Co., New York, p93(1950).

47. D. E. Reisner, R. W. Field, J. L. Kinsey, and H-L Dai, J. Chem. Phys., **80(12)**, 5968-5978(1984).

48. D. J. Clouthier, and D. A. Ramsay in **Ann. Rev. Phys. Chem.**, **34**, p31-58(1983).

Table I. Adiabatic Ionization Energies (eV) & Vibrational Frequencies (cm^{-1}) Observed

Ionic States	AIE[a] (eV)	$\nu_1, \omega_e x_e$ (cm^{-1})	$\nu_2, \omega_e x_e$ (cm^{-1})	$\nu_3, \omega_e x_e$ (cm^{-1})	$\nu_4, \omega_e x_e$ (cm^{-1})
$H_2CO^f\ \tilde{X}\ ^1A_1$		2782.5	1746.0	1500.2	1167.3
$H_2CO^+\ \tilde{X}\ ^2B_2$	10.8887(4)	2580.2(4.3)	1674.8, 19.0 (4.3)	1210.2, 6.1 (4.3)	777.1, 13.3 (4.3)
$\tilde{A}\ ^2B_1$	14.1024(2)		1250.5, 10.0 (4.3)	1487.7, 0.6 (4.3)	262.8[c] (4.3)
$\tilde{B}\ ^2A_1$	15.8375(3)		1304.5, 12.6 (4.3)	1304 (20)	
$\tilde{C}\ 2^2B_2$	16.2395(10)	1894.9[d], 11.3 (4.3)		1411.7[d], 12.5 (4.3)	

Ionic States	AIE[a] (eV)	$\nu_1, \omega_e x_e$ (cm^{-1})	$\nu_2, \omega_e x_e$ (cm^{-1})	$\nu_3, \omega_e x_e$ (cm^{-1})	$\nu_4, \omega_e x_e$ (cm^{-1})
$D_2CO^f\ \tilde{X}\ ^1A_1$		2055.8	1701.6	1105.7	938.0
$D_2CO^+\ \tilde{X}\ ^2B_2$	10.9076(4)	1948.2, 28.6 (4.3)	1656.7, 11.3 (4.3)	919.9, 31.1 (4.3)	648.1, 8.9 (4.3)
$\tilde{A}\ ^2B_1$	14.0999(5)	1064.5, 10.0 (4.3)	1281.6, 5.7 (4.3)		776.6[e] (4.3)
$\tilde{B}\ ^2A_1$	15.8425(2)		1311.1, 15.3 (4.3)	957.3, 3.4 (4.3)	
$\tilde{C}\ 2^2B_2$	16.4350(200)[b]	1604.4[d], 22.3 (4.3)	943.4[d], -12.7 (4.3)	818.7[d], -11.8 (4.3)	

(a) The absolute AIEs are accurate to ±3.0 meV as discussed in the main text. Other spectroscopic quantities, however, were obtained as line splittings, and can be reported to higher accuracy of ±0.5 meV (4.3 cm^{-1}). (b) This value is the best estimate. (c) the value of ν_4=1,0 splitting. (d) These values are estimates only. (e) The average value of ν_4 =2, 1, 0 splittings. (f) From ref. 47, 48. Number in parenthese indicate the uncertainties in the last digit.

TABLE II. Vibrational Levels of the $\tilde{X}\ ^2B_2$ State

H_2CO^+		D_2CO^+	
IE[a] (eV)	$\nu_1\nu_2\nu_3\nu_4$	IE[a] (eV)	$\nu_1\nu_2\nu_3\nu_4$
10.8887(3)	0000	10.9076(3)	0000
10.9834(5)	0001	11.1456(7)	1000
11.0748(6)	0002	11.3765(3)	2000
11.0380(8)	0010	11.1116(8)	0100
11.1858(4)	0020	11.3128(2)	0200
11.0940(2)	0100	11.0178(5)	0010
11.2946(5)	0200	11.1203(2)	0020
11.2086(3)	1000	10.9887(4)	0001
11.2483(8)	0110	11.0729(3)	0002
		11.1584(6)	0003
ν_n(n=1-4)(cm^{-1})	$\omega_e x_e$(cm^{-1})	ν_n(n=1-4)(cm^{-1})	$\omega_e x_e$(cm^{-1})
2580.2(4.3)		1948.2(4.3)	28.6(4.3)
1674.8(4.3)	19.0(4.3)	1656.7(4.3)	11.3(4.3)
1210.2(4.3)	6.1(4.3)	919.9(4.3)	31.1(4.3)
777.1(4.3)	13.3(4.3)	648.1(4.3)	8.9(4.3)
$\lvert C_{av}(t)\rvert^2$		$\lvert C_{av}(t)\rvert^2$	
$0.415e^{-0.153t} + 0.585e^{-0.0086t}$		$0.400e^{-0.0285t} + 0.600e^{-0.0095t}$	

(a). The absolute IEs are accurate to ±3.0 meV as discussed in the main text. Other spectroscopic constants, however, were obtained as line splittings, can thus be reported to a much higher accuracy ±0.5 meV(4.3 cm^{-1}).

(b). The $|C_{av}(t)|^2$ were presented as the summation of the initial and final decays of the form Ae^{-kt}. See main text for discussions.

TABLE III. Vibrational Levels of the $\tilde{A}\ ^2B_1$ State

IE[a] H_2CO^+ (eV)	$(\nu_1\nu_2\nu_3\nu_4)$	IE[a] H_2CO^+ (eV)	$(\nu_1\nu_2\nu_3\nu_4)$
14.1024(2)	0000	14.0999(5)	0000
14.1280(3)	0001	14.1366(4)	0001
14.2839(5)	0010	14.2925(2)	0002
14.4724(5)	0020	14.2283(6)	1000
14.6536(9)	0030	14.3659(4)	2000
14.2560(2)	0100	14.4874(8)	3000
14.4072(8)	0200	14.6204(8)	4000
14.5562(3)	0300	14.2604(6)	0100
14.7028(4)	0400	14.4163(9)	0200
14.8471(3)	0500	14.5723(2)	0030
14.9867(6)	0600	14.7282(5)	0040
15.1264(2)	0700	14.8750(2)	0050
15.2660(2)	0800	15.0309(4)	0060
15.3963(4)	0900	15.1763(1)	0070
14.2839(5)	0010	15.3282(1)	0080
14.4375(4)	0110	15.4755(9)	0090
14.5888(1)	0210	14.2283(6)	1000
14.7354(2)	0310	14.3865(8)	1100
14.8820(3)	0410	14.5425(1)	1200
15.0239(9)	0510	14.6984(4)	1300
15.1659(5)	0610	14.8497(8)	1400
15.3032(5)	0710	15.0034(2)	1500

Table III. continued

15.4382(3)	0810	15.1473(4)	1600
14.4724(5)	0020	15.2982(4)	1700
14.6213(9)	0120	15.4456(2)	1800
14.7726(6)	0220	14.2283(6)	2000
14.9192(7)	0320	14.3659(84	2100
15.0658(8)	0420	14.5149(9)	2200
15.2031(8)	0520	14.6686(3)	2300
15.3474(7)	0620	14.8199(7)	2400
14.6536(9)	0030	14.9736(1)	2500
14.8073(9)	0130	15.1207(9)	2600
14.9519(2)	0230	15.2694(2)	2700
15.0918(6)	0330	15.4156(4)	2800
		14.4874(8)	3000
		14.6411(2)	3100
		14.7924(6)	3200
		14.9438(2)	3300
		15.0959(2)	3400
		15.2407(8)	3500
		15.3881(6)	3600
		15.5330(4)	3700
		14.6204(8)	4000
		14.7718(2)	4100
		14.9185(1)	4200
		15.0749(3)	4300

Table III. continued

	15.2233(2)	4400
	15.3656(8)	4500
	15.5055(6)	4600
$\nu_2 = 1250.5$ (4.3), $\omega_e x_e = 10.0$ (4.3) cm^{-1}	$\nu_1 = 1064.5$ (4.3), $\omega_e x_e = 10.0$ (4.3) cm^{-1}	
$\nu_3 = 1487.7$ (4.3), $\omega_e x_e = 0.60$ (4.3) cm^{-1}	$\nu_2 = 1281.6$ (4.3), $\omega_e x_e = 5.7$ (4.3) cm^{-1}	
$\lvert C_{av}(t)\rvert^2$	$\lvert C_{av}(t)\rvert^2$	
$0.700e^{-0.400t} + 0.300e^{-0.006t}$	$0.700e^{-0.450t} + 0.300e^{-0.0013t}$	

(a). The accuracy of the IEs are ±1.0 meV for this state only, see main text for discussions. (b). See Table II. footnotes.

TABLE IV. Vibrational Levels of the $\tilde{B}\,^2A_1$ State

IE[a] H_2CO^+ (eV)	$\nu_1\nu_2\nu_3$	IE[a] D_2CO^+ (eV)	$\nu_1\nu_2\nu_3$
15.8375(2)	000	15.8425(2)	000
15.9963(1)	010	15.9631(8)	001
16.1541(1)	020	16.0823(7)	002
16.3079(5)	030	16.1986(1)	003
16.4593(2)	040	16.3111(9)	004
16.6071(1)	050	16.4229(3)	005
16.7506(6)	060	16.5422(4)	006
		16.6558(8)	007
		16.0029(1)	010
		16.1603(5)	020
		16.3111(9)	030
		16.4649(5)	040
		16.6062(1)	050
		16.7497(6)	060
		16.1235(7)	011
		16.2740(5)	021
		16.4240(5)	031
		16.5826(7)	041
		16.7324(6)	051
		16.2412(8)	012
		16.3972(6)	022
		16.5502(9)	032
		16.6954(2)	042

Table IV. continued

	16.3575(3)	013
	16.5127(7)	023
ν_2 = 1304.5 (4.3), $\omega_e x_e$ = 12.6 (4.3) cm^{-1}	ν_2 = 1311.1 (4.3), $\omega_e x_e$ = 15.3 (4.3) cm^{-1}	
	ν_3 = 957.3 (4.3), $\omega_e x_e$ = 3.4 (4.3) cm^{-1}	
$\lvert C_{av}(t)\rvert^2$	$C_{av}(t)\rvert^2$	
$0.550e^{-0.100t} + 0.450e^{-0.001t}$		

(a). See table II. footnotes.

TABLE V. Vibrational Levels of the $\tilde{C}\ 2^2B_2$ State

IE[a] H_2CO^+ (eV)	$(\nu_1\nu_2\nu_3)$	IE[a] D_2CO^+ (eV)	$(\nu_1\nu_2\nu_3)$
16.2395(3)	000	16.4350(200)	000 (?)
16.4811(5)	100	16.5036(5)	001
16.7065(3)	200	16.6973(4)	101
16.9304(2)	300	16.8863(2)	201
17.1581(2)	400	17.0799(9)	301
17.3832(1)	500	17.2524(2)	401
17.6041(3)	600	17.4272(1)	501
17.8163(5)	700	17.5972(7)	601
16.4130(2)	001	16.6341(6)	100
16.5833(8)	002	16.7310(9)	110
16.7506(6)	003	16.8680(2)	120
16.5316(1)	010	16.9938(3)	130
16.792(8)	110	17.1300(6)	140
17.0449(5)	210	17.2621(4)	150
17.2958(7)	310	17.3873(8)	160
17.5304(2)	410	17.5216(9)	170
17.7450(5)	510	16.8381(5)	020
16.63914	020	16.9181(5)	021
16.8145(2)	021	17.0322(9)	022
16.9825(1)	022	17.1525(8)	023
17.1428(4)	023	17.2621(4)	024
17.3123(5)	024	17.3732(2)	025
17.4631(5)	025	17.4909(8)	026

TABLE V. continued

	17.6086(7) 027
ν_1 = 1894.9 (4.3), $\omega_e x_e$ = 11.3 (4.3)cm^{-1}	ν_1 = 1604.4 (4.3), $\omega_e x_e$ = 22.3 (4.3) cm^{-1}
ν_2 = ? cm^{-1}	ν_2 = 943.4 (4.3), $\omega_e x_e$ = -12.7 (4.3) cm^{-1}
ν_3 = 1411.7 (4.3), $\omega_e x_e$ =12.5 cm^{-1}	ν_3 = 818.7 (4.3), $\omega_e x_e$ = -11.8(4.3) cm^{-1}
$\lvert C_{av}(t)\rvert^2$	$\lvert C_{av}(t)\rvert^2$
$.99e^{-0.200t} + 0.01e^{-0.015t}$	$0.90e^{-0.185t} + 0.10e^{-0.035t}$

a. See footnotes of table II., also see main text for discussions.

Figure Captions:

Figure 1. The full spectra of formaldehyde and deuterated formaldehyde with a resolution of 11 meV FWHM. The designation of the ionic states assumes that the ions have C_{2V} symmetry.

Figure 2. The photoelectron spectra of the $\tilde{X}\ 1^2B_2$ state of the H_2CO^+ and D_2CO^+, with a resolution of 11 meV FWHM. The vibrational progressions are labeled according to the C_{2V} geometry and 2_0^1 stands for the transition

$M^+ (\nu_2 = 1) + e^- \leftarrow M (\nu_2 = 0) + \hbar\,\omega$

following standard spectroscopic notations.

Figure 3. The vibrational autocorrelation functions of the $\tilde{X}\ 1^2B_2$ states of H_2CO^+ and D_2CO^+ after all the corrections have been made. The calculated $|C_{av}(t)|^2$ functions are plotted as dotted lines.

Figure 4. The photoelectron spectra of the $\tilde{A}\ ^2B_1$ states of H_2CO^+ and D_2CO^+. Notations are the same as in Fig. 2. Rotational cooling, combined with the high resolution obtained by this study, enabled the multiplet vibrational fine structures to be fully resolved here for the first time.

Figure 5. The vibrational autocorrelation function calculated for the $\tilde{A}\ ^2B_1$ state of H_2CO^+. Note the beat pattern was caused by multimode excitation and a small spin-orbit splitting for this state. Shown at the bottom is the correlation function, after all corrections have been made.

Figure 6. The vibrational autocorrelation function calculated for the $\tilde{A}\ ^2B_1$ state of D_2CO^+. Note the beat pattern was caused by multimode excitation and a small spin-orbit splitting for this state. Shown at the bottom is the

correlation function after all corrections have been made.

Figure 7. The photoelectron spectra of the $\tilde{B}\,^2A_1$ and $\tilde{C}\,2^2B_2$ states of H_2CO^+ and the $\tilde{B}\,^2A_1$ state of D_2CO^+ with a resolution of 11 meV FWHM. Note the FWHM of the peaks in this band are only about 12 meV, indicating very effective rotational relaxation in the supersonic expansion.

Figure 8. The vibrational correlation functions calculated for the $\tilde{B}\,^2A_1$ states of H_2CO^+ and D_2CO^+. The correlation function clearly shows that there is only one vibrational mode excited in H_2CO^+.

Figure 9. The photoelectron spectrum of the $\tilde{C}\,2^2B_2$ state of D_2CO^+ with a resolution of 11 meV FWHM. Even with very effective rotational cooling and current high resolution measurements, the complexity of this band still eludes our analysis. The band structure observed is characteristic of a repulsive state.

Figure 10. The vibrational correlation function calculated for the $\tilde{C}\,2^2B_2$ state of H_2CO^+ and D_2CO^+ after all corrections were made. The main feature of the correlation function is the extremely fast decay and loss of correlation, indicating ultrafast intramolecular dynamics processes.

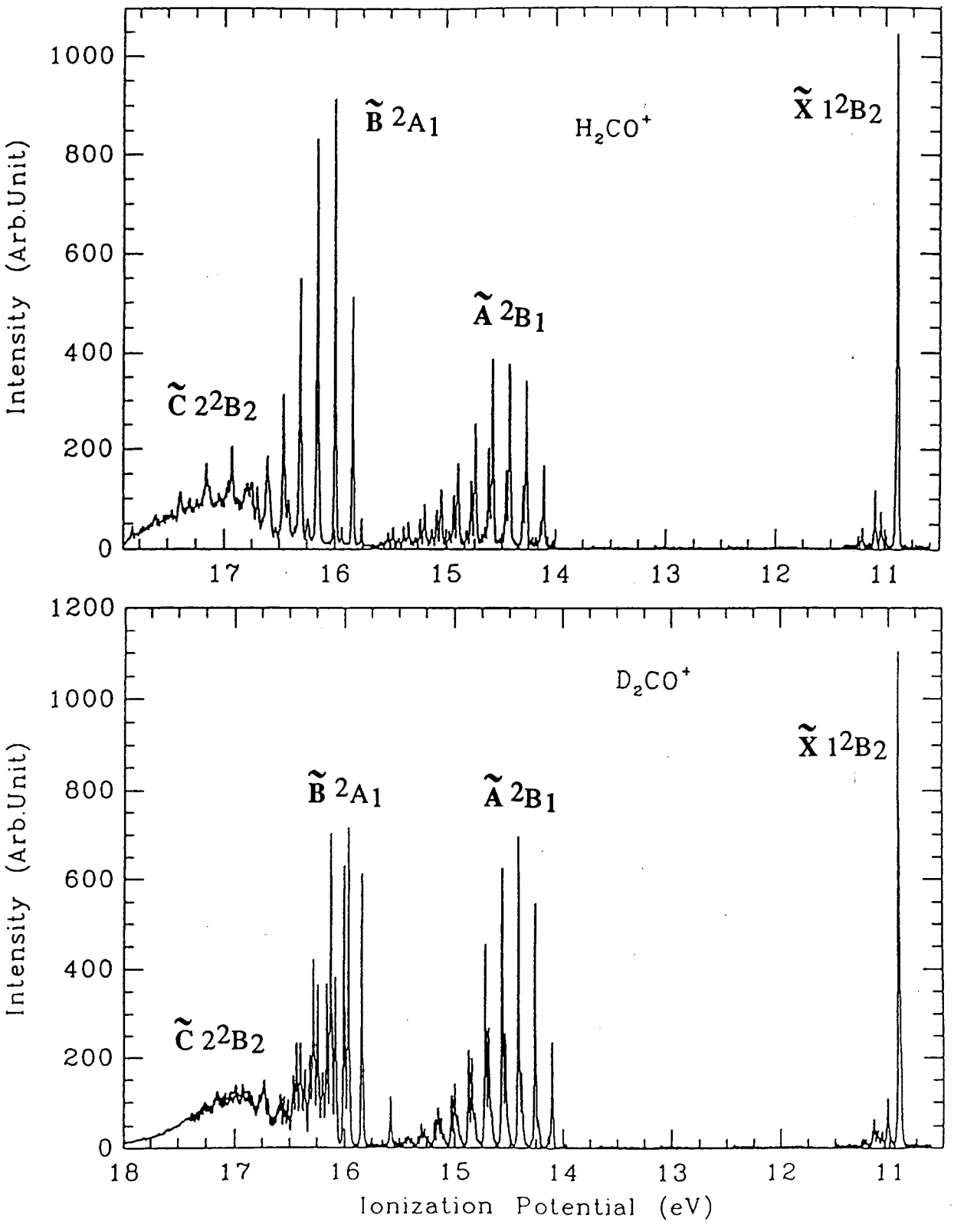
Intensity (Arb.Unit)
1000
800
600
400
200
0
$\tilde{B}\,^2A_1$
H_2CO^+
$\tilde{X}\,^1{}^2B_2$
$\tilde{A}\,^2B_1$
$\tilde{C}\,^2{}^2B_2$
17
16
15
14
13
12
11
1200
1000
800
600
400
200
0
D_2CO^+
$\tilde{X}\,^1{}^2B_2$
$\tilde{B}\,^2A_1$
$\tilde{A}\,^2B_1$
$\tilde{C}\,^2{}^2B_2$
18
17
16
15
14
13
12
11
Ionization Potential (eV)

Figure 1.

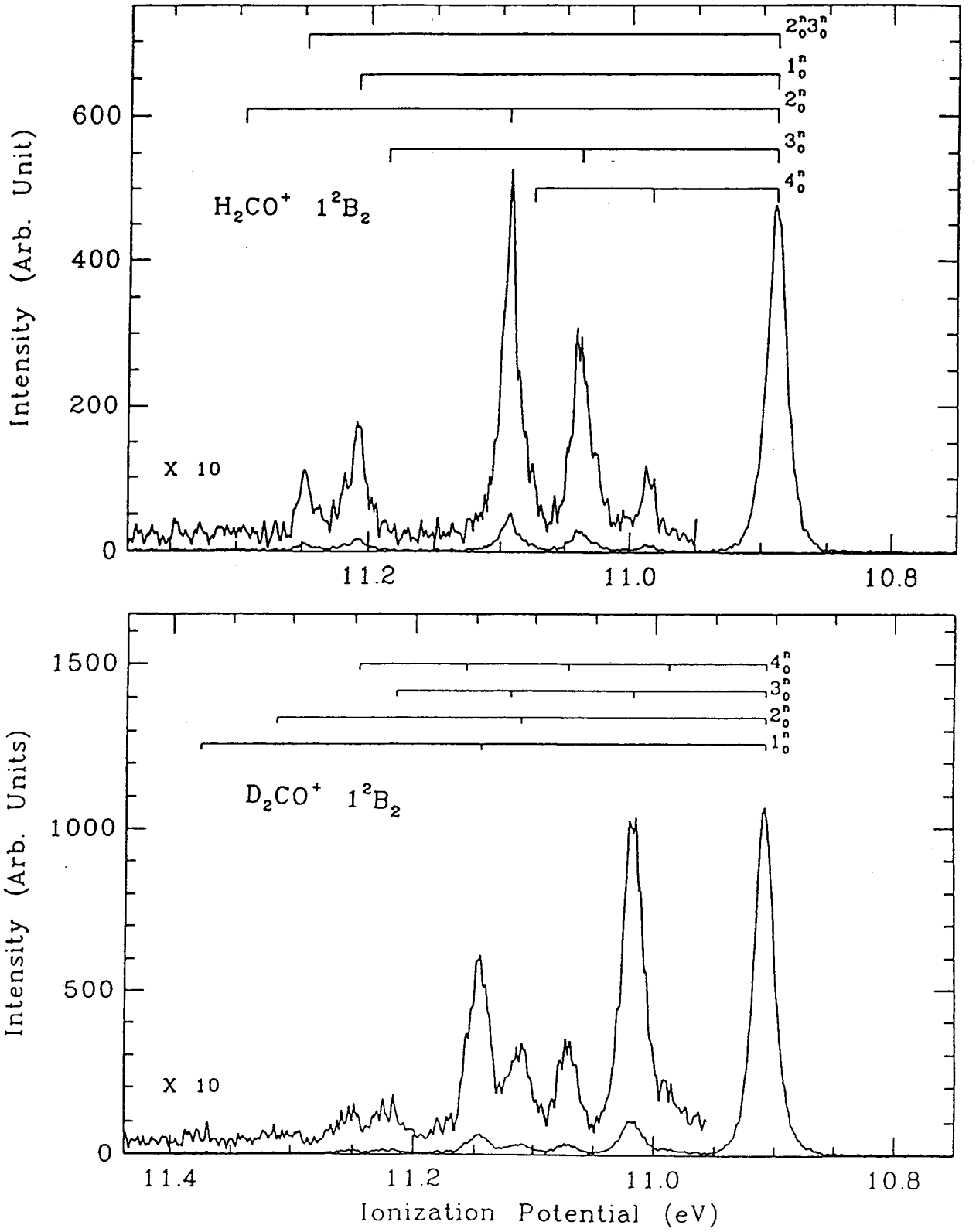
$2_0^n3_0^n$
1_0^n
2_0^n
3_0^n
4_0^n
H_2CO^+ 1^2B_2
X 10
Intensity (Arb. Unit)
600
400
200
0
11.2
11.0
10.8
4_0^n
3_0^n
2_0^n
1_0^n
D_2CO^+ 1^2B_2
X 10
Intensity (Arb. Units)
1500
1000
500
0
11.4
11.2
11.0
10.8
Ionization Potential (eV)

Figure 2

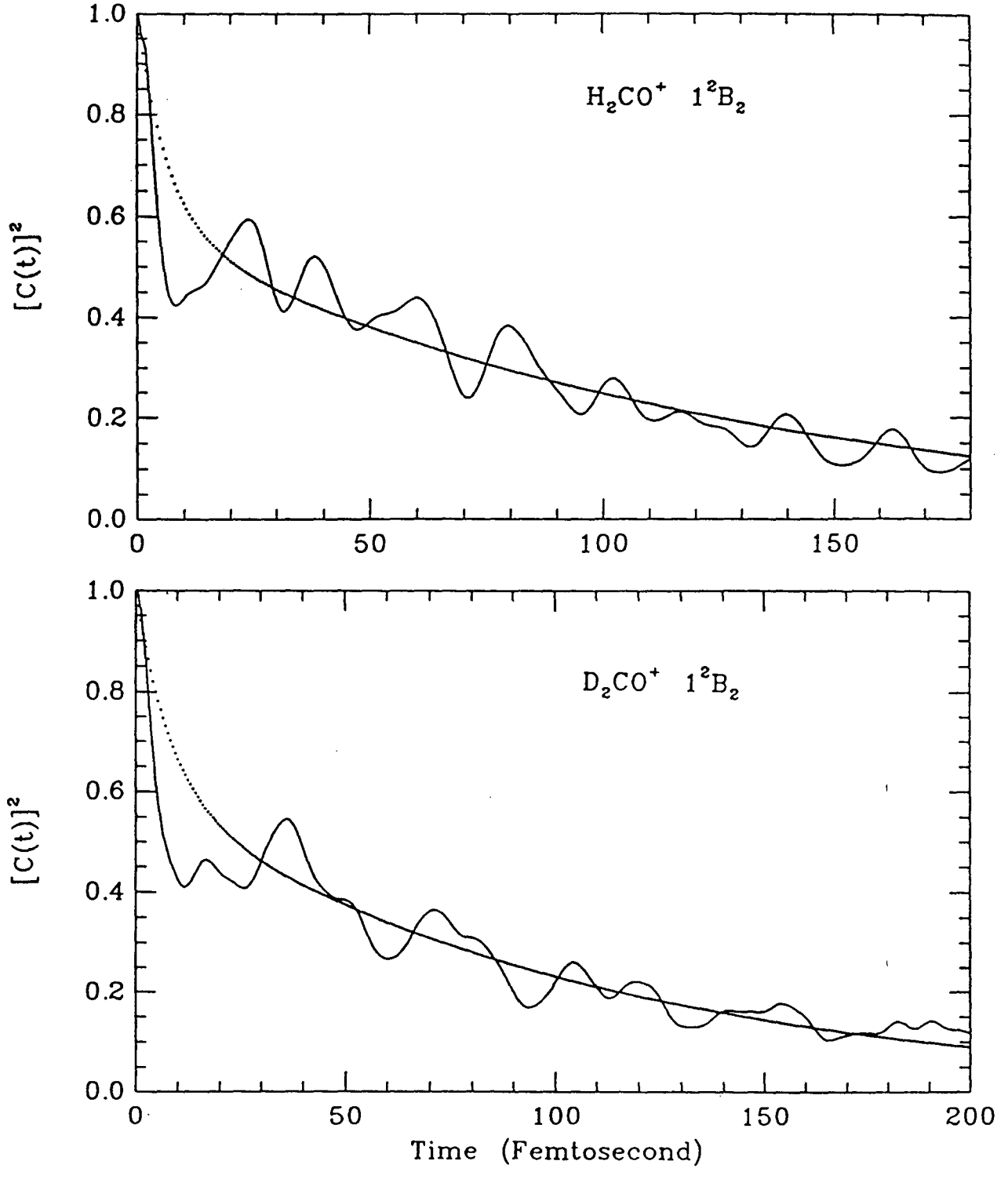
1.0
0.8
0.6
0.4
0.2
0.0
[C(t)]²
H₂CO⁺ 1²B₂
0
50
100
150
D₂CO⁺ 1²B₂
200
Time (Femtosecond)

Figure 3

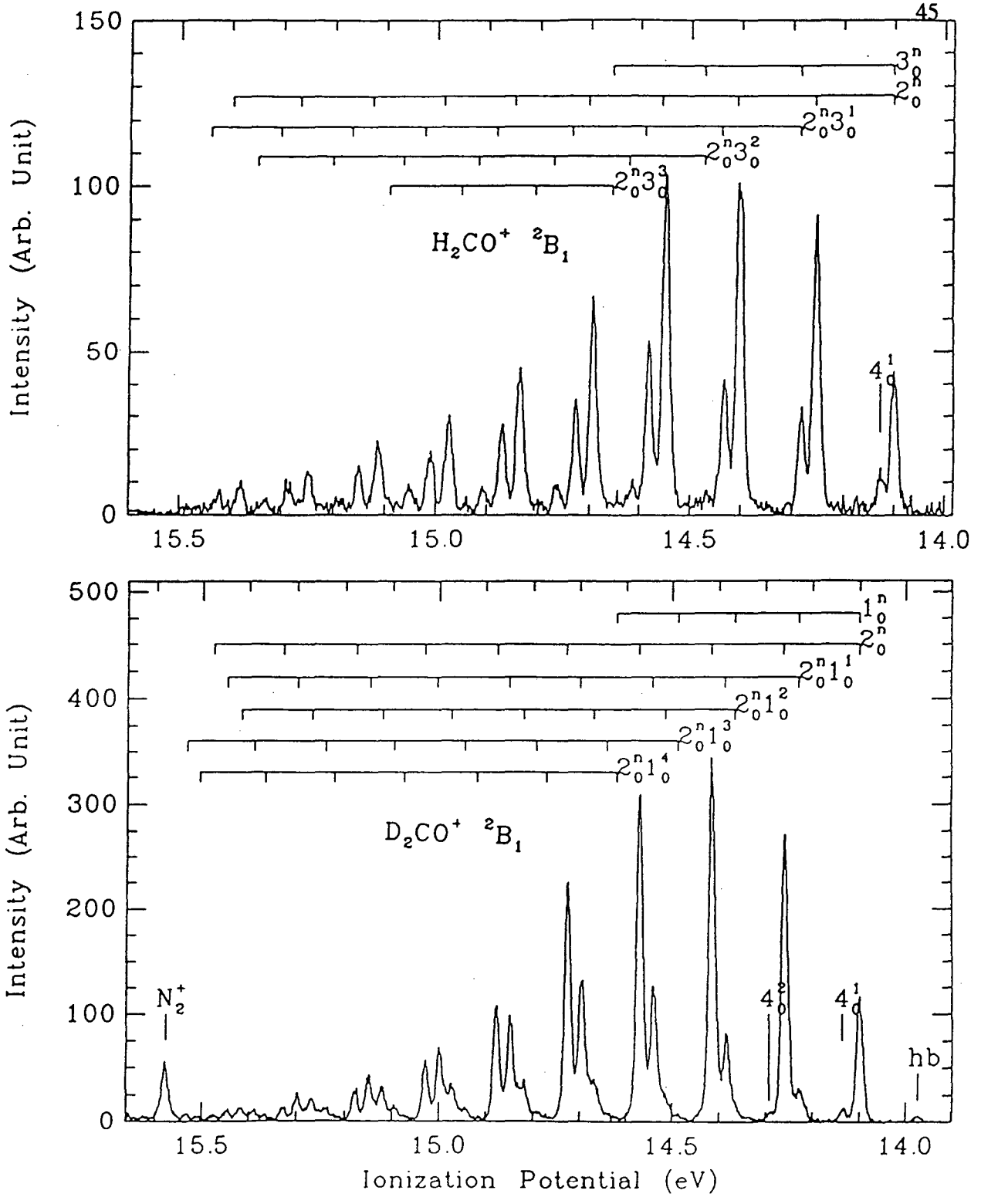
150
100
50
0
Intensity (Arb. Unit)
H_2CO^+ $^2B_1$
3_0^n
2_0^n
$2_0^n3_0^1$
$2_0^n3_0^2$
$2_0^n3_0^3$
4_0^1
15.5
15.0
14.5
14.0
500
400
300
200
100
0
Intensity (Arb. Unit)
D_2CO^+ $^2B_1$
1_0^n
2_0^n
$2_0^n1_0^1$
$2_0^n1_0^2$
$2_0^n1_0^3$
$2_0^n1_0^4$
N_2^+
4_0^2
4_0^1
hb
15.5
15.0
14.5
14.0
Ionization Potential (eV)

Figure 4

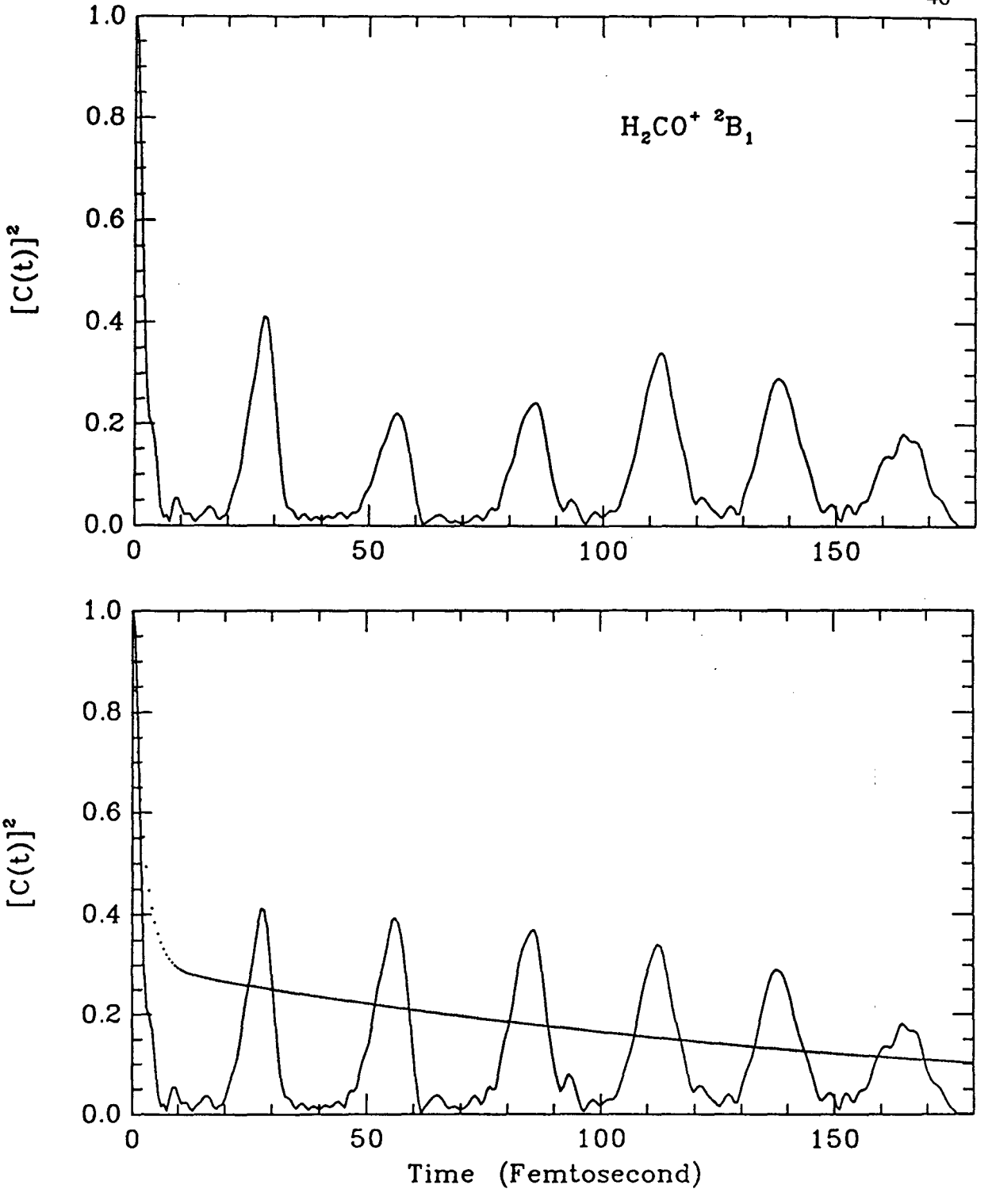
1.0
0.8
0.6
0.4
0.2
0.0
[C(t)]²
H₂CO⁺ ²B₁
0
50
100
150
1.0
0.8
0.6
0.4
0.2
0.0
[C(t)]²
0
50
100
150
Time (Femtosecond)

Figue 5

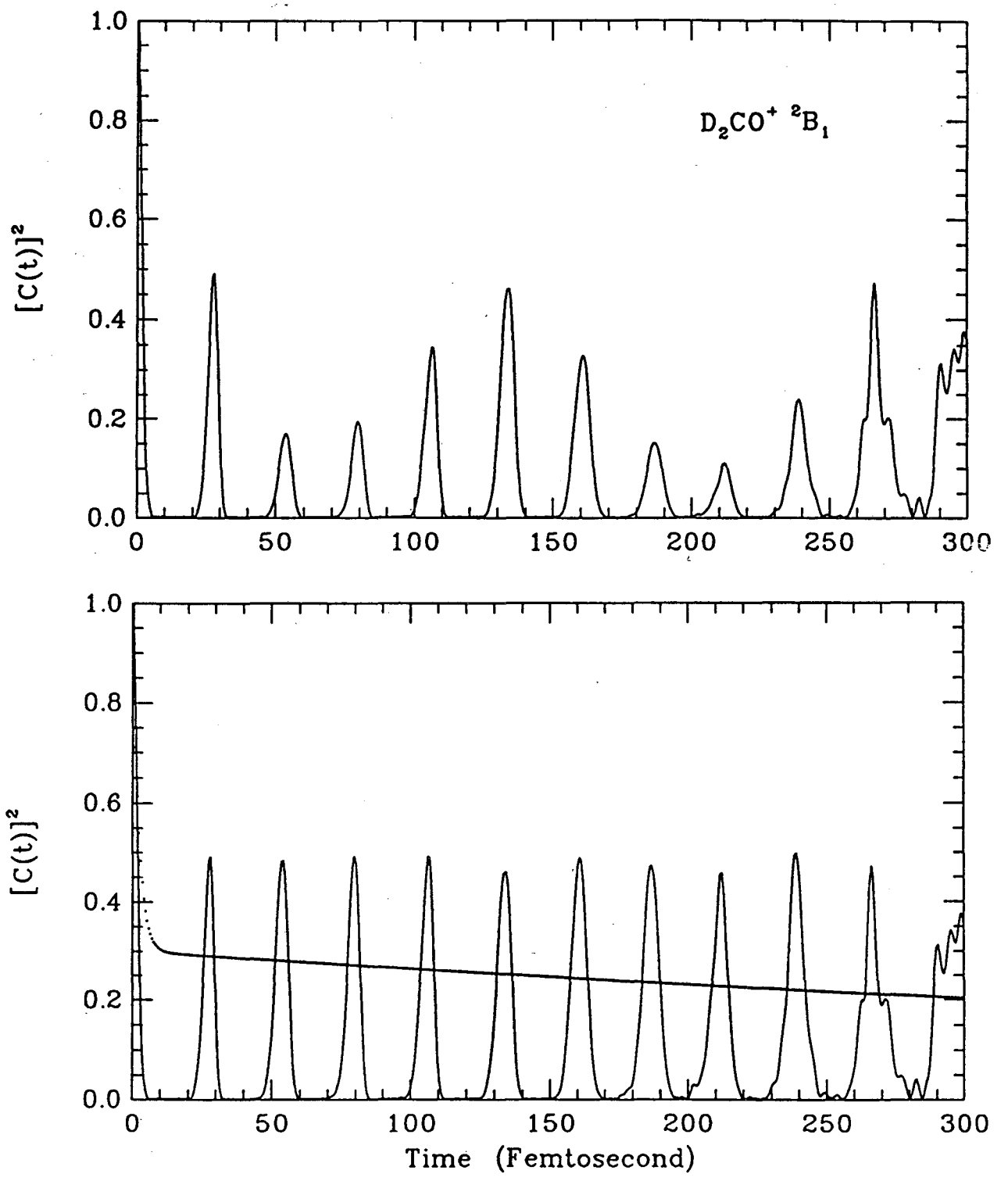
$D_2CO^+ \ ^2B_1$
$[C(t)]^2$
1.0
0.8
0.6
0.4
0.2
0.0
0
50
100
150
200
250
300
Time (Femtosecond)

Figure 6

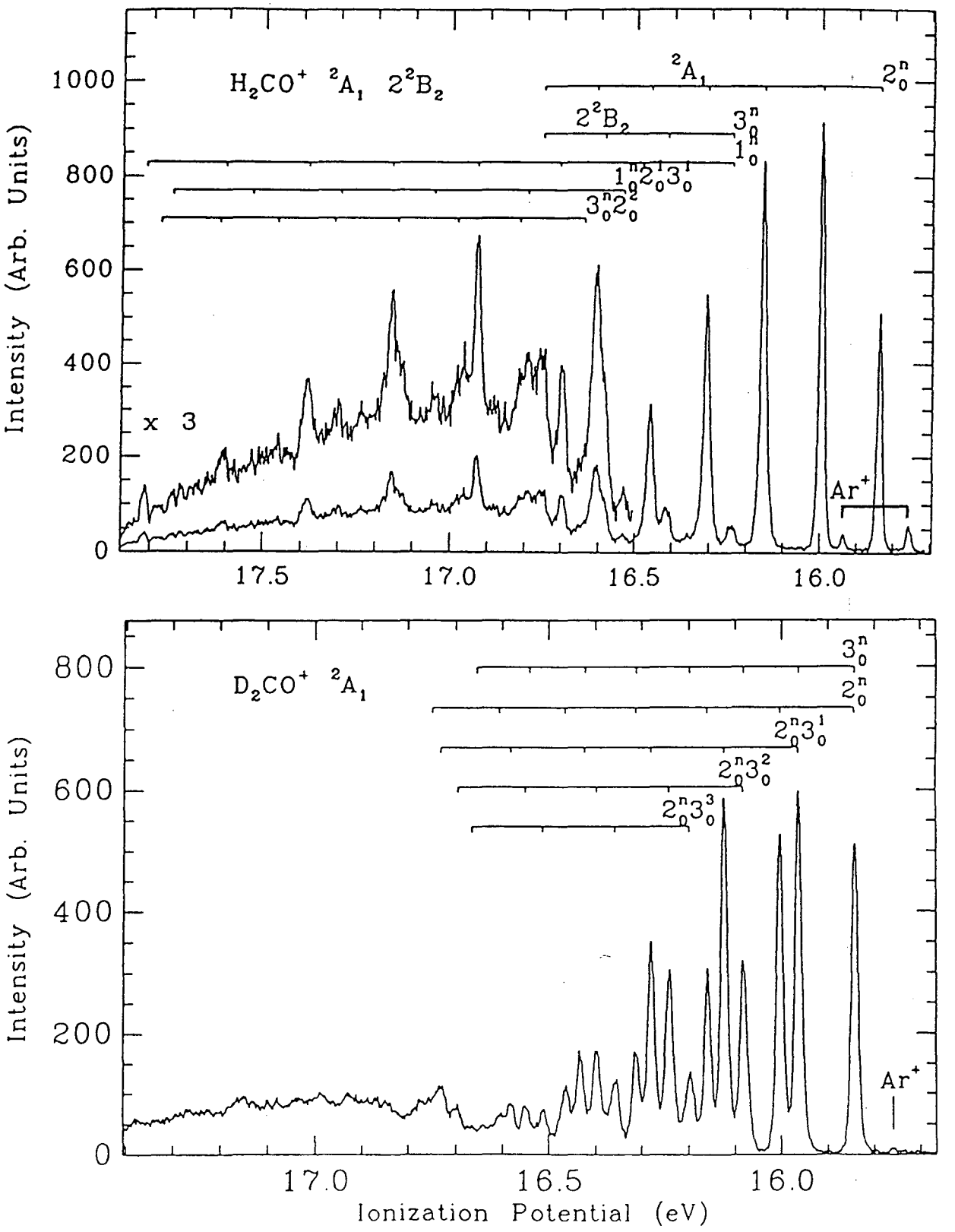
H2CO+ 2A1 2 2B2
2A1
2 0 n
2 2B2
3 0 n
1 0
1 0 n 2 0 1 3 0 1
3 0 n 2 0 2
x 3
Ar+
Intensity (Arb. Units)
1000
800
600
400
200
0
17.5
17.0
16.5
16.0
D2CO+ 2A1
3 0 n
2 0 n
2 0 n 3 0 1
2 0 n 3 0 2
2 0 n 3 0 3
Ar+
Intensity (Arb. Units)
800
600
400
200
0
17.0
16.5
16.0
Ionization Potential (eV)

Figure 7

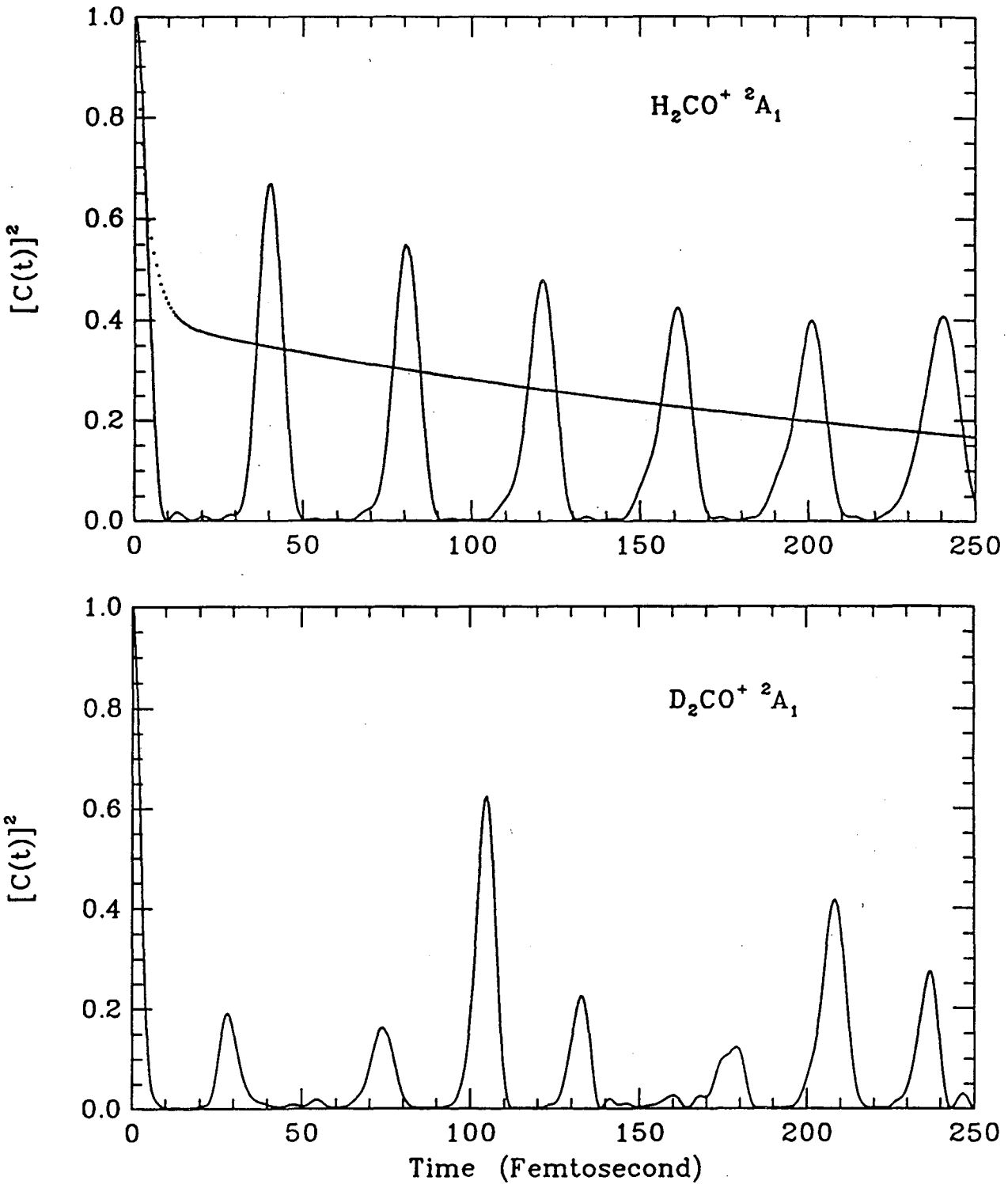
1.0
0.8
0.6
0.4
0.2
0.0
[C(t)]²
H₂CO⁺ ²A₁
0
50
100
150
200
250
D₂CO⁺ ²A₁
Time (Femtosecond)

Figure 8

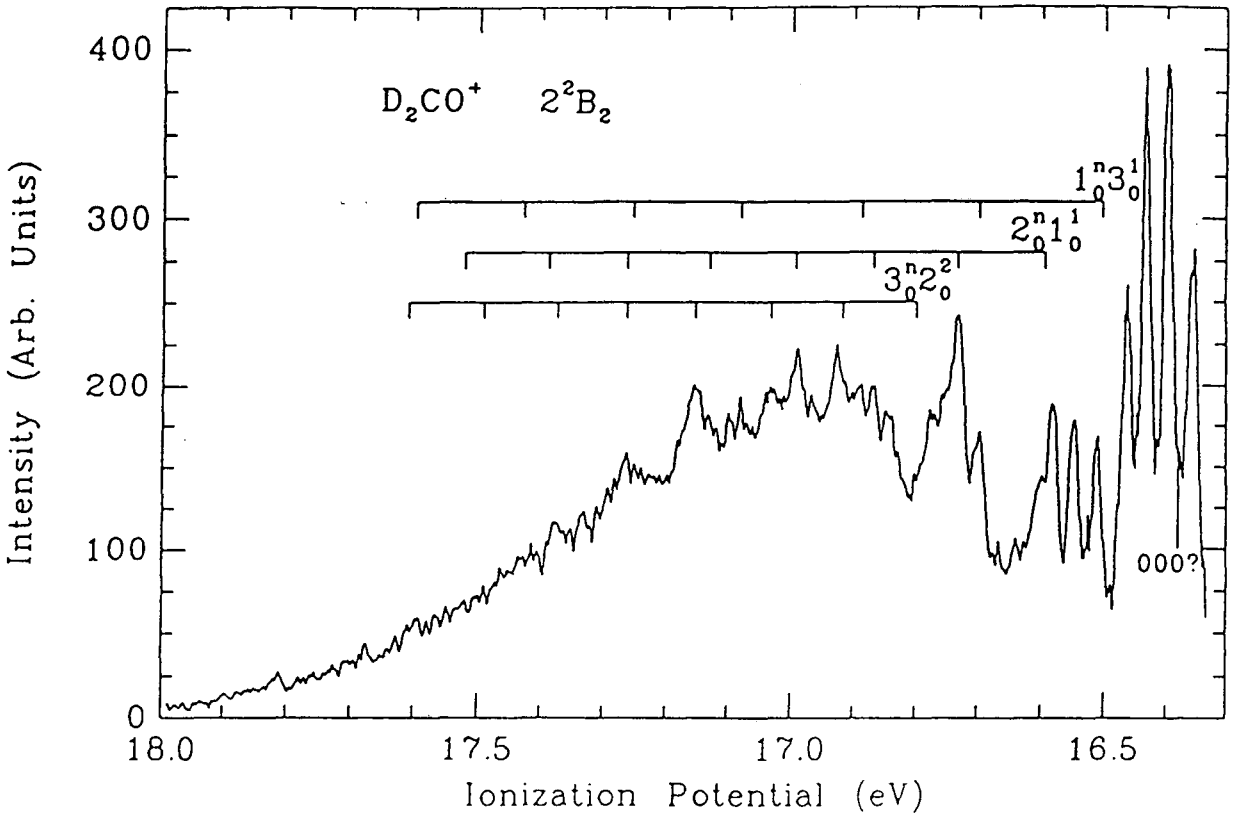
400
300
200
100
0
Intensity (Arb. Units)
D_2CO^+ 2^2B_2
$1_0^n3_0^1$
$2_0^n1_0^1$
$3_0^n2_0^2$
000?
18.0
17.5
17.0
16.5
Ionization Potential (eV)

Figure 9

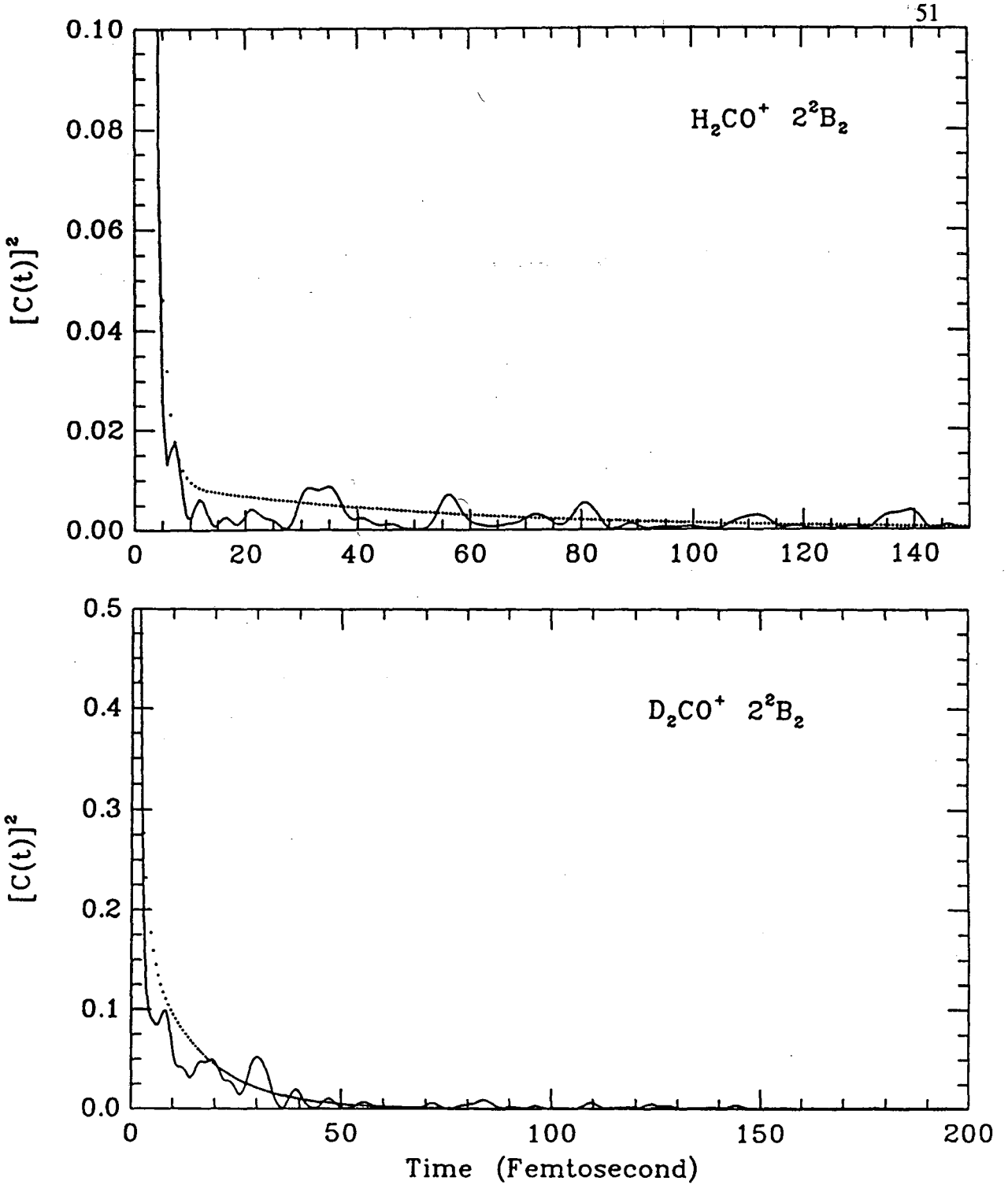
0.10
0.08
0.06
0.04
0.02
0.00
[C(t)]²
H₂CO⁺ 2²B₂
0
20
40
60
80
100
120
140
0.5
0.4
0.3
0.2
0.1
0.0
[C(t)]²
D₂CO⁺ 2²B₂
0
50
100
150
200
Time (Femtosecond)

Figure 10.

LAWRENCE BERKELEY LABORATORY
UNIVERSITY OF CALIFORNIA
TECHNICAL INFORMATION DEPARTMENT
BERKELEY, CALIFORNIA 94720